Polycomb repressive complex 2 coordinates with Sin3 histone deacetylase complex to epigenetically reprogram genome-wide expression of *effectors* and regulate pathogenicity in *Magnaporthe oryzae*

Zhongling Wu[1,§], Jiehua Qiu[2,§], Huanbin Shi[2], Chuyu Lin[1], Jiangnan Yue[1], Zhiquan Liu[2], Wei Xie[1], Yanjun Kou[2*] and Zeng Tao[1*]

[1]State Key Lab of Rice Biology, Ministry of Agriculture Key Laboratory of Molecular Biology of Crop Pathogens and Insects, Institute of Biotechnology, Zhejiang University, Hangzhou, China.

[2]State Key Lab of Rice Biology, China National Rice Research Institute, Hangzhou, China

[§] These authors contributed equally.

[*] Correspondence: taozeng@zju.edu.cn (Z.T.)，kouyanjun@caas.cn (Y.K.).

Running head: Reprogramming of *effectors* during *Magnaporthe oryzae*–rice interaction

Abstract

The strict suppression and reprogramming of gene expression are necessary at different development stages and/or in response to environment stimuli in eukaryotes. In Rice *Magnaporthe oryzae* pathosystem, *effectors* from pathogen are kept transcriptionally silenced in the vegetative growth stage and are highly expressed during invasive growth stage to adapt to the host environment. However, the mechanism of how such *effectors* are stably repressed in the vegetative stage and its roles during rice blast infection remain unclear so far. Here, we showed that all subunits of Polycomb Repressive Complex 2 are required for such repression by direct H3K27me3 occupancy and pathogenic process in *M. oryzae*. Suppression of polycomb-mediated H3K27me3 causes an improper induction of *effectors* during vegetative growth thus simulating a host environment. Notably, the addition subunit P55 not only acts as the bridge to connect with core subunits to form a complex in *M. oryzae*, but also recruits Sin3 histone deacetylase complex to prompt H3K27me3 occupancy for stable maintenance of transcriptional silencing of the target genes in the absence of PRC1. In contrast, during invasive growth stage, the repressed state of *effectors* chromatin can be partially erased during pathogenic development resulting in transcriptional activation of effectors therein. Overall, Polycomb repressive complex 2 coordinates with Sin3 histone deacetylase complex to epigenetically reprogram genome-wide expression of *effectors,* which act as molecular switch to memorize the host environment from vegetative to invasive growth, thus contributing to the infection of rice blast.

Key words: rice blast; PRC2; histone deacetylation; Sin3-HDAC; transcriptional reprogramming

Introduction

Organisms need to reprogram gene expression properly in different development stages or environment stimuli, which suppressing unnecessary genes is the most of important process (Cavalli and Heard, 2019, Netea et al., 2016). Stable maintenance of repressed gene expression states is achieved partly by the propagation of specific chromatin modifications (Cavalli and Heard, 2019). Evolutionary conserved polycomb repressive complexes (PRC) plays a vital role in such repression and contributes to facultative heterochromatin (Schuettengruber et al., 2017, Wiles and Selker, 2017, Margueron and Reinberg, 2011). PRC is involved in various biological processes, including maintaining cellular and tissue identity in multicellular organisms and regulating phase transitions in plants (Margueron and Reinberg, 2011, Blackledge et al., 2015). In mammals and higher plants, there are two main polycomb group complexes, PRC1 and PRC2 (Lanzuolo and Orlando, 2012). PRC1, including Pc, Ph, and Psc, compacts chromatin and catalyzes the monoubiquitylation of histone H2A. PRC2, including core subunits proteins, Ezh (Kmt6), Su(z)12, Esc (Eed) and additional subunits RbAp48/Nurf55 (P55), catalyzes the methylation of histone H3 at lysine 27 (Wiles and Selker, 2017, Schuettengruber et al., 2017). The core PRC2 complex is conserved from *Drosophila* to mammals and higher plants, while the PRC1 complex is not evolutionarily conserved. Notably, PRC1 has not been identified in fungi so far (Margueron and Reinberg, 2011, Ridenour et al., 2020).

In the fungi kingdom, disruption of PRC usually reprograms genome-wide gene expression, leading to abnormal growth and reduced pathogenicity (Ridenour et al., 2020, Wiles and Selker, 2017). In *Fusarium graminearum*, deletion of core subunits of PRC2 resulted in the complete loss of H3K27me3 modification, ~2,500 genes up-regulation, as well as severe defects in growth and pathogenicity (Connolly et al., 2013). In *Magnaporthe oryzae*, deletion of *KMT6* eliminated all H3K27me3 modifications, resulted in a decrease in sporulation and highly reduced pathogenicity in wheat and barley (Pham et al., 2015). In *Neurospora crassa*, loss of core subunits also abolished

all H3K27me3 modification, but only accompanied by slight growth defects (Jamieson et al., 2013). In the yeast *Cryptococcus neoformans*, loss of *EZH2, Eed1* or additional subunit *Bnd1* removed all H3K27me3 modification, while loss of the novel accessory component *Ccc1* resulted in regional reduction and relocalization of H3K27me3 modification on the chromosome (Dumesic et al., 2015). In symbiotic fungus *Epichloe festucae*, H3K27me3 coupled with H3K9me3 controls expression of symbiosis-specific genes, such as genes related to alkaloid bioprotective metabolites (Chujo and Scott, 2014). Although many studies have been done on the PRC complex in fungi, how the PRC2 effectively regulates gene expression and stably maintains the repressive H3K27me3 modification on the target chromatin in the absence of PRC1 remains largely unclear (Ridenour et al., 2020, Wiles and Selker, 2017).

During plant–pathogen interaction, pathogens have evolved multiple layer of strategies to invade host effectively, including secreting effectors to modulate rice immunity and ensure progressive infection (Fouche et al., 2018). Reprogramming the expression of the *effectors* by the pathogen is often used as an effective strategy to invade the host (Fouche et al., 2018). In addition, recent studies showed that transcriptional polymorphism with *effectors* contributes to the adaption of pathogenic microbes to environmental changes and co-evolution with host (Fouche et al., 2018). In the soybean root rot pathogen *Phytophthora sojae*, occupancy of H3K27me3 at *Avirulence* gene *Avr1b* leads to transcriptional silencing and fails to induce the *Rps1b* mediated disease resistance (Wang et al., 2020). However, in the vegetative growth stage, how to maintain the stable suppression of expression of *effectors* remains unclear.

Rice blast, caused by *M. oryzae*, is the most devastating disease of rice and threatens food security worldwide. In *M. oryzae*–rice interaction, the majority of the *effectors* are kept transcriptional silencing or expressed relatively low in the vegetative growth stage (Dong et al., 2015, Sharpee et al., 2017, Jeon et al., 2020), but are de-repressed during invasive growth stage (Dong et al., 2015, Jeon et al., 2020). During preparing our manuscript, a really good study found that H3K27 dynamics associate

with altered transcription of *in planta* induced genes in *M. oryzae* (Zhang et al., 2021). Here, we not only find that histone modification H3K27me3 is required for genome-wide transcriptional silencing of *effectors* during vegetative growth stage in *M. oryzae*, but also present the detailed and novel mechanism beyond these findings. First, all subunits of PRC2, are required for H3K27me3-meditating polycomb silencing on the *effectors* and pathogenicity, which the addition subunit P55 acts as the bridge to connect with the core subunits to form a complex in *M. oryzae*. Furthermore, P55 recruits Sin3 histone deacetylase complex to coordinate with PRC2 and prompts H3K27me3 occupancy on the target chromatin. During invasive growth stage, the repressed chromatin state on the *effectors* can be partially "erased", resulting in the transcriptional activation of *effectors*. In addition, we also reveal the important role of Sin3 histone deacetylase complex in transcriptional reprogramming the genome-wide expression of *effectors*, as well as in pathogenicity.

Results

Kmt6, as well as other PRC2 subunits, is indispensable for H3K27me3 modification in *M. oryzae*

In *M. oryzae*, Kmt6 (*MGG_00152*) was reported as the writer of H3K27me3 modification which is associated with altered transcription of *in planta* induced genes in *M. oryzae* (Pham et al., 2015, Zhang et al., 2021). However, how H3K27 trimethylation achieve stably transcriptional silencing of *effectors* during vegetative growth remains largely unknown. To answer this question, Δ*kmt6* was created in the wild-type (WT) *M. oryzae* strain B157. As reported, the expression levels of representative *effectors* during vegetative growth stage exhibited significant increased expression levels than that of the WT (Figure 1a)(Khang et al., 2010, Mosquera et al., 2009, Sharpee et al., 2017). To verify whether the increased transcriptional expression of *effectors* would enhance accumulation and secretion of effectors during vegetative growth stage, the *BAS4-GFP* construct was introduced into the Δ*kmt6* strain. As shown in the Figure 1b, the Bas4-GFP signal was clearly evident in the conidia, and the apical

and subapical regions of the hyphae of the Δ*kmt6* mutant, but was not detectable in those of the WT. These results indicated that removal of H3K27me3 modification leads to untimely expression of *BAS4* during vegetative growth stage similar with that found naturally during invasive growth stage (Figure 1b).

Polycomb-group genes were first identified in *Hox* regulation in *Drosohpila* and are usually assembled with Polycomb repressive complex 1(PRC1) and PRC2 (Blackledge et al., 2015, Ridenour et al., 2020). To identify the candidate PRC1 and other PRC2 subunits in *M. oryzae*, BLASTp was used to search for the orthologs from *M. oryzae* 70-15 genomes (taxid: 242507) with the query sequences from *Neurospora crassa, Arabidopsis thaliana,* and *Drosophila melanogaster* (Table S1). Three unique PRC2 core subunits, Kmt6 (MGG_00152), Eed (MGG_06028), Suz12 (MGG_03169), and one additional subunit P55 (MGG_07323) were obtained, while no PRC1 subunits was hit even by low stringency BLAST in *M. oryzae* (Table S1, Figure S1).

To investigate whether Kmt6, Eed, Suz12 and P55 form a complex, we first fused these proteins with GFP and examined their subcellular localization in *M. oryzae*. As shown in the Figure 2a, all these subunits were co-localized Hoechst-stained nuclei, suggesting that these components may form a complex in the nucleus like PRC2 in other species (Figure 2a). Then, yeast two-hybrid assay was conducted to test whether these subunits are physically associated *in vitro*. *KMT6*, *Suz12*, *Eed* and *P55* were cloned to the prey and bait vectors respectively. These results showed that the additional subunit P55 interacts with other three core subunits, and Kmt6 interacts with Eed in the yeast cells (Figure 2b). Furthermore, co-immunoprecipitation assays with strains expressing *Eed-GFP* and *Kmt6-Flag*, *P55-GFP* and *Kmt6-Flag*, *P55-GFP* and *Suz12-Flag*, *P55-GFP* and *Eed-Flag* respectively further confirmed these interactions *in vivo* (Figure 2c-f). Taken together, these results suggested that Kmt6, Eed, Suz12 and P55 form a complex, and P55 serves as the bridge to connect the PRC2 components.

To explore whether Eed, Suz12, and P55 are indeed required for H3K27me3 modification, deletion mutants of *Suz12*, *Eed* and *P55* were created by homolog recombination in the WT. Subsequently, the protein levels of histone lysine methylation were detected with specific antibodies using Western blotting assay. The levels of H3K27me3 were almost undetectable in the Δ*kmt6*, Δ*eed* and Δ*suz12* mutants, while the level of H3K27me3 in the Δ*P55* still retained half level of the WT (Figure 2f), which indicated that P55 is not essential for H3K27me3 modification as the core subunits. Furthermore, the decreased levels of H3K27me3 in the mutants were completely restored in the complementary strains respectively (Figure 2f). Meanwhile the levels of H3K4me3 and H3K36me3 had no obvious change in all aforementioned strains by comparing with that of WT (Figure S2). We conclude that Kmt6, Suz12 and Eed are fully and specifically required for H3K27me3 modification, while P55 partially contributes to H3K27me3 modification.

All PRC2 subunits are required for mycelia growth, conidiation, and pathogenicity in *M. oryzae*

To investigate the function of PRC2 complex in *M. oryzae*, mycelia growth and conidiation were assessed in the Δ*kmt6*, Δ*eed*, Δ*suz12*, Δ*p55*, as well as their complementary strains. Similar with the Δ*kmt6*, Δ*suz12* and Δ*eed* strains exhibited decreased mycelia growth and dramatically reduced conidiation, which had similar phenotype with recent report (Zhang et al., 2021) (Figure 3a-c). Notably, Δ*p55* had more severe phenotype in the mycelia growth (Figure 3a-b), suggesting that P55 had wider functions beside for acting as the bridge in the PRC2 complex. These results indicated that H3K27me3 is required for the mycelia growth and conidiation in *M. oryzae.*

To analyse the function of PRC2 components in pathogenicity, conidia of the WT, mutant and complementary strains were collected and then inoculated on the susceptible rice cultivar CO39 (*Oryza sativa*). As the number of conidia from mutants

highly reduced (15-25% of the WT) (Figure 3c), low concentration of conidia (5×10^4/mL) were used in the rice seedling infection assay. Compared with WT, which caused the characteristic spindle-shaped blast lesions with grey centres, mutant strains formed relative fewer and restricted lesions (Figure 3d-e). To further decipher these observations, the appressoria formation on the inductive hydrophobic surface and rice sheath were investigated. Although no obvious change in appressoria formation at 24 hpi (hour post inoculation) was found in the mutant strains (data not shown), the invasive growth displayed significant difference between the mutants and WT (Figure 3f). Nearly 90% appressoria from the WT strain successfully penetrated the rice sheath, while only 60% appressoria from the deletion mutants were capable of penetration (Figure 3f) at 40 hpi. Moreover, the formation of secondary invasive hyphae in the mutant strains was less than that of WT. These results indicated that H3K27me3 is necessary for penetration and invasive hyphal growth.

Core subunits of PRC2, together with P55, suppress genome-wide gene expression, including *effectors*, at vegetative growth stage

To explore the roles of H3K27me3 in the transcriptional regulation in *M. oryzae*, high-throughput sequencing (RNA-seq) was performed using the vegetative mycelia with three biological repeats. As H3K27me3 always contributes to transcriptional silencing on target genes, the mutant strains would be expected to enrich with high ratio of de-repressed genes. As expected, totally 19.2%, 18.6%, 20.1% and 15.4% of genome-wide genes were identified as up-regulated genes (UEG) with equal or greater than 2-fold change ($Log_2 > 1$, $P<0.05$), while only 5.3%, 6.0%, 8.8% and 3.3% of genes were identified as down-regulated genes (DEG) in the Δ*kmt6*, Δ*eed*, Δ*suz12* and Δ*p55* strains respectively ($Log_2 <-1$, $P<0.05$) (Figure 4a). As the core subunits of PRC2, Δ*kmt6*, Δ*eed* and Δ*suz12* shared 80-86% overlaps (2144 genes) in their UEG (Figure S3a). The high ratio of co-regulated genes further indicated that Kmt6, Eed and Suz12 function in the same complex. Moreover, the predominant roles of de-repressed regulation in the mutants of core subunits suggested that H3K27me3 modification played conserved

roles as transcriptional repressors in *M. oryzae* (Figure 4a). Although P55 was thought as additional subunit which was different from other three core subunits, there was no obvious difference in the gene sets between the Δ*kmt6*-UEG and Δ*p55*-UEG strains (P=0) (Figure S3b). These results further confirmed that core subunits of PRC2, together with P55, function in the same complex and regulate similar biological processes.

To explore the detailed biological process involved in PRC2, Gene Ontology (GO) analysis was conducted with Δ*kmt6*-UEG. Biological process as "interaction with host *via* secreted protein" were significantly enriched (Figure S3c). This was consistent with our hypothesis that H3K27me3 modification contributes to suppress the expression of *effectors* at vegetative growth stage. To further address this question, gene sets of putative genome-wide *effectors*, including 134 (only 124 *effectors* had reads in our RNA-seq) and 247 (only 246 *effectors* had reads in our RNA-seq) *effectors* from two different literatures respectively, were extracted for further analysis (Sharpee et al., 2017, Dong et al., 2015). Compared with the WT, nearly 51.6% (64/124) and 42.7% (105/246) *effectors* exhibited significantly increased expression in the Δ*kmt6* strain (Figure 4b and S4). To preclude the specificity of strain background, similar analysis was performed with the Δ*kmt6* mutant in the Guy11 background. The ratio of up-regulated *effectors* in the Δ*kmt6* either in B157 or Guy11 background were significantly enriched with similar tendency (Figure 4b and S5a-c). We concluded that H3K27me3 is specifically required in the suppression of *effectors* during vegetative growth stage in *M. oryzae*.

In addition, loss of H3K27me3 modification not only activated the expression of *effectors*, but also activated some infection-specific genes such as those encoding cutinases and cell-wall degrade enzymes, which indicated that the absence of H3K27me3 could partially mimic host-derived signal. Therefore, we compared the gene sets between Δ*kmt6*-UEG and UEG from 36 hpi and 72 hpi *in planta* from published RNA-seq respectively (Jeon et al., 2020). The results showed that 30.1%

(820/2654) of 36 hpi-UEG and 33.1% (778/2353) 72 hpi-UEG were significantly overlapped with Δ*kmt6*-UEG (Figure S6a-b).

H3K27me3 occupancy is associated with increased transcription in the PRC2 mutants

To further depict whether H3K27me3 directly deposits on the chromatin of *effectors*, we attempted to map the genome-wide H3K27me3 occupancy using chromatin immunoprecipitation assay followed by high-throughput sequencing (ChIP-seq) in the WT and Δ*kmt6* strains. The intensity of H3K27me3 occupancy in the Δ*kmt6* mutant was barely detectable (Figure S7a), which was consistent with the role of Kmt6 as the H3K27me3 writer in *M. oryzae.* Compared with the Δ*kmt6* mutant, totally 1082 significant peaks were identified in the WT ($Log_2 > 1$, $P < 0.05$), which were corresponded to 1033 genes and mainly spread within gene bodies (Supplemental Figure 7a-b). To verify whether Δ*kmt6*-UEG were directly associated with the loss of H3K27me3 occupancy, the gene sets between Δ*kmt6*-UEG under low or high threshold and H3K27me3-marked genes were compared. With low threshold ($Log_2 > 1$, $P < 0.05$), 23.5% (645 of 2743) of Δ*kmt6*-UEG were marked with directly H3K27me3 occupancy (Figure S7c). while with stringent threshold ($Log_2 > 3$, $P < 0.05$)，40.1% (532 of 1327) of Δ*kmt6*-UEG were marked with H3K27me3 (Figure S7c). Together, the de-repressed genes in the Δ*kmt6* are highly correlated with the absence of H3K27me3 occupancy.

Next, GO analysis was conducted with H3K27me3-occupancy genes. Biological process “interaction with host via protein secreted” were highly enriched (Figure 4c), similar with the results from the Δ*kmt6*-UEG. Significantly, 26.7% (33 of 124) and 19.9% (49 of 246) of effectors were directly marked with H3K27me3 modification (Figure 4d and S7d). The chromatin of representative *effectors* as *BAS3*, *BAS4*, *SPD5* and *SPD10* enriched with H3K27me3 modification in the WT but nearly undetectable in the Δ*kmt6* mutant (Figure 4e). Consistently, the increased expression of examined *effectors* accompanied with almost undetectable H3K27me3 level in the Δ*kmt6* with ChIP-qPCR

assay (Figure 1a and 4f). In addition, gene sets of 36 hpi-UEG and 72 hpi-UEG *in planta* were also highly marked with H3K27me3 (Figure S6a-b) and the chromatin state of four cutinases loci was validated with ChIP-qPCR (Figure S7e). These results further indicated that the H3K27me3 modification directly associates with transcriptional silencing on the *effectors* and infection-specific genes.

P55 recruits Sin3 histone deacetylase complex to form a co-suppression complex

How PRC2 performs stable transcriptional silencing on the target chromatin in the absence of PRC1 remains unclear (Ridenour et al., 2020, Margueron and Reinberg, 2011). As a chromatin assembling factor and histone-binding WD40-repeat proteins, ortholog of the additional subunit P55 was reported to associate with other co-suppression complex to conduct transcriptional silencing in other organisms (Mehdi et al., 2016, Gu et al., 2011). As the additional subunit of PRC2 in *M. oryzae*, P*55* acts as the bridge to connect other core subunits together and Δ*p55* exhibited more severe phenotype than other mutants in our experiments. We postulated that P55 may recruit other co-suppression machinery to help PRC2 to stably maintain polycomb silencing. To address this possibility, P55 was fused to the bait vector and putative histone deacetylases were cloned individually in the prey vector for yeast-two-hybrid assays. As a result, we found that P55 interacted with four components of Sin3 histone deacetylases complex in yeast two-hybrid assays (Figure 5a). Sin3 histone deacetylases complex has been well characterized in yeast and other organisms (Huang et al., 2019, Grzenda et al., 2009, Adams et al., 2018), which the core components of Sin3 histone deacetylase complex includes histone deacetylase Hos2 (MGG_01633)(Lee et al., 2019), major regulatory protein Sin3 (MGG_13498), other subunits Sap18 (MGG_05680) and Sap30 (MGG_11142) in *M. oryzae*. Moreover, Sap30 interacted with other three components as Hos2, Sin3 and Sap18 in yeast which indicated that these components function in the same complex (Figure S8a). Coimmunoprecipitation assays with the strains expressing *P55-GFP*/*Sin3-Flag*, and *P55-GFP*/*SAP18-Flag* further confirmed that P55 is physically associated with Sin3-HDAC *in vivo* (Figure

5b-c).

To explore the function of Sin3-HDAC in *M. oryzae*, the deletion mutants of *Sin3*, *Sap18* and *Sap30* were created. Among these mutants, Δ*sin3* exhibited severe phenotype similar to Δ*p55*, including decreased fungal growth, severely reduced conidiation, as well as highly reduced pathogenicity (Figure 5d-h). To investigate whether Sin3-HDAC contributes to the histone deacetylation activity *in vivo*, the global levels of histone acetylation were checked in the WT and Δ*sin3* strains. Among the examined acetylated residues, at least the levels of H3K4ac, H3K27ac and H4K5ac were significantly increased in the Δ*sin3* strain than that of WT (Figure 6a and S8b). The increased level of H3K4ac in the Δ*sin3* was further confirmed by ChIP-seq assay. The global H3K4ac occupancy in the Δ*sin3* was significantly increased than that of WT, which further confirmed that Sin3-HDAC has histone deacetylation activity in *M. oryzae* (Figure S8c). As loss of histone deacetylation would accompany with genome-wide gene activation, we conducted RNA-seq with total RNA extracted from the Δ*sin3* and WT strains. In the vegetative growth stage, deletion of *Sin3* dramatically altered the expression of nearly 38% of genome-wide genes compared with WT. Totally, 3049 genes were up-regulated ($Log_2 > 1$, $P < 0.05$), and 1454 genes were down-regulated ($Log_2 < -1$, $P < 0.05$) which implied that *Sin3* also acts as a transcriptional repressor similar with P55 and Kmt6 (Figure 6b). Based on these results, we conclude that Sin3-HDAC contributes to histone deacetylation activity and acts as a transcriptional repressor to regulate genome-wide gene expression in *M. oryzae*.

Sin3-HDAC co-operates with PRC2 to prompt transcriptional repression on the target genes

To explore the transcriptional correlation between Sin3-HDAC and PRC2, the transcriptional profiles of the Δ*sin3* and Δ*kmt6* strains were compared. A total of 1489 genes which were 54.3% of Δ*kmt6*-UEG and 48.8% of Δ*sin3*-UEG were significantly overlapped (P=0) (Figure 6c). To further address whether Sin3-HDAC contributes to

H3K27me3-mediated transcriptional silencing, we investigated whether Δ*sin3*-UEG are enriched with H3K27me3 occupancy. The results showed that with lower stringent threshold ($Log_2 > 1$, $P < 0.05$), 16.2% (495 of 3049) of Δ*sin3*-UEG were occupied with H3K27me3 modification. While with higher stringent threshold ($Log_2 > 3$), 26.8% (396 of 1478) of Δ*sin3*-UEG were directly associated with H3K27me3 occupancy (Figure 6d). Meanwhile, enhanced H3K4ac and H4K5ac levels were also observed in the Δ*kmt6* and other PRC2 deletion mutants (Figure S8d). These results suggested that Sin3-mediated histone deacetylation contributes to PRC2-mediated transcriptional silencing on the target genes.

Next, GO analysis was conducted with Δ*sin3*-UEG. The term of "interaction with host via protein secreted" were highly enriched (Figure S9), which was similar with the results from RNA-seq in the Δ*kmt6* strain, indicating that Sin3-HDAC and PRC2 may coordinately regulate the expression *of effectors.* Therefore, the putative effectome that includes 124 and 246 predicted members were further investigated in the Δ*sin3*-UEG (Dong et al., 2015, Sharpee et al., 2017). The results showed that 49.2% (61 of 124, 121/246) predicted *effectors* exhibited significantly increased expression in the Δ*sin3* strain (Figure 6e). To verify these results from RNA-seq analysis, RT-qPCR was performed with three independent repeats in the WT and Δ*sin3* strains. Consistently, the expression of the *BASs* and *SPDs* in Δ*sin3* were significantly de-repressed in the vegetative growth stage (Figure 6f). In addition, a precocious and significant induction of *BAS4-GFP* signal was found in the conidia and vegetative hyphae of Δ*sin3*, thus indicating that deletion of *Sin3* leads to Bas4 accumulation and secretion during the vegetative growth stage (Figure S10).

Taken together, these results conclude that P55 recruits Sin3-HDAC as a co-repressor complex to maintain stably transcriptional silencing on the target genes, including a large scale of *effectors,* during vegetative growth in *M. oryzae*.

H3K27me3 modification is "erased" from the chromatin of *effectors* loci during *M.*

390 ***oryzae*–rice interaction**

391 To address whether the activated expression of *effector*s during infection stage is
392 associated with reduced H3K27me3 occupancy, we attempted to conduct ChIP-qPCR
393 to check H3K27me3 enrichment on chromatin of the *effectors* as *BAS3*, *BAS4*, *SPD5*
394 and *SPD10* using *in vivo* infected rice leaves with the WT strain. The results showed
395 that expression of four tested *effectors* was significantly induced from 24 hpi to 72 hpi
396 (Figure 7a). Subsequently, 72 hpi-infection leaves were collected for ChIP assay.
397 Compared with the mycelia, the relative H3K27me3 abundance of 72 hpi-infection
398 leaves dramatically reduced at the chromatin regions of *BAS3*, *BAS4* and *SPD5*, except
399 *SPD10*, which indicated that the activated expression of *effectors* would be partially
400 caused by removing of H3K27me3 modification (Figure 7b).
401
402 **Discussion**
403
404 In this study, we have revealed how H3K27me3 modifies the expression of genome-
405 wide *effectors* and contributes to infection of *M. oryzae*. Suppression of H3K27me3
406 improperly activated the expression of *effectors* in the vegetative growth stage, as well
407 as highly decreased pathogenicity. We also revealed a new mechanism that the
408 additional subunit P55 acts as the bridge to connect core subunits to form a complex
409 and recruits Sin3-HDAC to prompt H3K27me3 occupancy on the *effectors*, therefore
410 stably maintain polycomb silencing in the absence of PRC1. During invasive growth
411 stage, the repressed chromatin state on *effectors* is partially “erased”, subsequently the
412 expression of *effectors* is activated to promote the infection of *M. oryzae*.
413
414 Epigenetic modification was correlated with genome plasticity and stability, help
415 pathogen effective adaption to host environments (Chadha and Sharma, 2014, Wang et
416 al., 2020, Cavalli and Heard, 2019). In *M. oryzae*, epigenetic modification as histone
417 (de)methylation and (de)acetylation have been extensively explored in different
418 biological processes such as infection structure morphogenesis, developmental
419 transition and autophagy. Histone deacetylases Tig1 and Hos2 regulate infectious

growth and asexual development in *M. oryzae* (Ding et al., 2010, Lee et al., 2019). H3K4 methyltransferase Set1 contributes to appressorium formation, conidiation and pathogenicity with transcriptional activation on the infection-related genes (Pham et al., 2015). Histone acetyltransferase Gcn5 negatively regulates light-induced autophagy and conidiation through acetylated the autophagy protein Atg7 (Zhang et al., 2017). *MoSNT2* plays key roles in infection-associated autophagy through recruiting histone deacetylase complex on the target chromatin (He et al., 2018). Recently, Zhang et al. elucidated that H3K27 dynamics associate with altered transcription of *in planta* induced genes, including *effectors*, in *M. oryzae* (Zhang et al., 2021). In our study, we found that all core subunits of PRC2, together with the additional subunit P55, are required for H3K27me3-meditating polycomb silencing on the *effectors* in the vegetative growth stage and pathogenicity. Our results also revealed that histone modification H3K27me3, coordinately mediated by PRC2 and Sin3 histone deacetylase complex, directly suppresses most of the genome-wide *effectors* expression. Previous studies suggested that pathogen *effectors* are rapidly evolved and especially distributed in regions with high genome plasticity. In *M. oryzae*, *effectors* do not have common motifs or conserved *cis*-elements that contribute to their adaptability to host environment (Sanchez-Vallet et al., 2018, Dong et al., 2016). Thus, H3K27me3 seems to preferentially modify the poorly conserved or newly evolved *effectors* to "guard" the genome through transcriptional silencing (Dong et al., 2015, Sanchez-Vallet et al., 2018, Fouche et al., 2018). Whenever necessary, such as in response to the host environment, fungal pathogens redistribute H3K27me3 and evoke transcriptional activation, then the activated *effectors* help the pathogens to better adapt to and colonize their host (Fouche et al., 2018).

Polycomb silencing has been extensively studied in multicellular organisms, which is conserved from *Drosophila* to mammals and higher plants, as well as in the fungi kingdom (Margueron and Reinberg, 2011, Ridenour et al., 2020, Wiles and Selker, 2017, Schuettengruber et al., 2017). The core subunits Kmt6, Suz12 and Eed are necessary for H3K27me3 modification and transcriptional silencing (Wiles and Selker,

2017). However, the role of *P55*, the additional subunit of PRC2, remains obscure in fungi. In *F. graminearum*, the homolog of subunit p55 is not involved in H3K27me3 modification (Ridenour et al., 2020). In *N. crassa*, *P55* (*NPF*) is critical for H3K27me3 in a region-dependent manner (Jamieson et al., 2013). In our research, we found that *P55* plays a critical role in H3K27me3-mediated transcriptional silencing in *M. oryzae.* First, P55 acts as the bridge to connect three core components together. Second, disruption of *P55* largely reprograms gene expression, which significantly overlaps with those of Δ*kmt6* and is directly associated with H3K27me3 occupancy. Third, P55 recruits Sin3-HDAC to form the co-suppression complex with PRC2.

The Sin3-HDAC corepressor complex is usually associated with a large number of DNA-binding transcription factors or corepressors to achieve specific and timely regulation of local chromatin and transcription (Grzenda et al., 2009). In Sin3 histone deacetylase complex, Sap30 serves as the bridge and stabilizing molecule and Sap18 also involves in the apoptosis and splicing associated protein (ASAP) complex (Adams et al., 2018, Grzenda et al., 2009, Julia I. Qüesta, 2016). In our study, we found that P55 recruits Sin3 histone deacetylase complex to form co-suppression complex. Furthermore, Sin3 functions as a transcriptional repressor and participates in the *effectors*-related biological process similar to PRC2. All these results suggested that Sin3-HDAC would promote H3K27me3 occupancy and facilitate PRC2 machinery in stably maintaining condensed chromatin status and achieving gene silencing coordinately. In addition, it is possible that Sin3-associated transcription factors or corepressors help H3K27me3 recruitment properly (Adams et al., 2018). This finding not only provides a plausible explanation that PRC2 could stably maintain transcriptional silencing in the absence of PRC1, but also elucidates the molecular clue of transcription output caused by crosstalk between histone methylation and (de)acetylation in *M. oryzae*.

Establishment and maintenance H3K27me3 to local chromatin depends on histone "reader" and series of *trans*/*cis*-regulatory factors which act in corporate or alone

(Kassis and Brown, 2013, Xiao et al., 2017). One of the best example of epigenetically reprograming is regulation of floral repressor *Flowering Locus C* (*FLC*) under vernalization (winter cold exposure) in model plant *Arabidopsis* (Luo and He, 2020). In our study, we found that the silenced effectors would be de-repressed with reduced H3K27me3 occupancy during invasive growth stage. Consistent with *FLC* as molecular switch to "remember" vernalization in *Arabidopsis* (Luo and He, 2020), transcriptional reprogramming of some specific *effectors* in *M. oryzae* may act as the molecular switch to "remember" the host environment. However, it is still unknown how the repressed chromatin is "erased" and how the activated state is established during invasive growth stage. Given the destined *effectors*, it is worthy to further elucidate these detailed mechanisms.

Materials and Methods

Fungal strains and culture conditions

The *M. oryzae* WT strain B157 and Guy11 were used as background strain to obtain transformants in this study, which were kind gifts from the Indian Institute of Rice Research (Hyderabad, India). All the WT in this study is B157, except for those marked with Guy11. For growth assessment of *M. oryzae*, strains were grown on the prune agar medium (PA) for 7 d (Kou et al., 2017). For conidiation, strains were grown on CM medium at 28℃ in the dark for 2 d, followed by growth under continuous lights for 5 d.

Plasmid construction

To create the deletion mutants of *KMT6*, *Eed*, *Suz12*, *P55*, *Sin3*, *Sap18* and *Sap30*, the standard one-step gene replacement strategy was used in this study. Briefly, approximate 1-kb of 5'UTR and 3'UTR regions were amplified and ligated sequentially to the flanking of *Hygromycin*，*Sulf* or *Bar* gene cassette in the *pFGL821* (Addgene, 58223), *pFGL820* (Addgene, 58222) or *pFGL822* (Addgene, 58225) respectively (Kou et al., 2017). The sequences of plasmids were confirmed by sequencing and subsequently introduced into the B157 strain by *Agrobacterium tumefaciens* mediated

transformation (ATMT). To generate the localization and complementary vectors, the *eGFP* and *TrpC* terminator were cloned to *pFGL820* to obtain *pFGL820-GFP-TrpC* terminator. The fragments containing about 1.5-kb of promotor and coding region were amplified (primers listed in Table S2) and then cloned to *pFGL820-GFP-TrpC* terminator. After conformed by sequencing, the resultant plasmids were introduced into corresponding deletion mutants respectively by ATMT.

To generate the constructs of *pRP27-KMT6-Flag*, *pRP27-Suz12-Flag* and *pRP27-P55-Flag* for co-immunoprecipitation assay, the coding sequence were cloned to *pFGL822-pRP27-Flag* or *pFGL820-pRP27-eGFP*. The confirmed plasmids were introduced into deletion mutants respectively by ATMT. Primers used in the experiments were listed in Table S2.

Live cell imaging and image processing

The CM cultivated hypha were stained with 100 μg/mL Hoechst 33342 (Sigma, 14533) for 20 min to visualize nuclei. Live cell epifluorescence microscopy imaging was performed with LSM700 (CarlZeiss Inc.), using the requisite conditions established for detecting GFP or Hoechst signals. Image processing was performed using image J (http://fiji.sc/wiki/index.php/Fiji). These experiments were conducted with two independent repeats.

Appressorial formation assay

For appressoria formation assay, conidia were harvested from 7-d-old cultures and resuspended in sterile water at a concentration of 10^5 conidia per mL. 10 μL droplets of the conidial suspension were inoculated on the hydrophobic plastic cover slips and incubated in high humidity at room temperature (Kou et al., 2017). The appressoria were quantified at 24 hpi. Photographs were taken with an Olympus BX53 wide field microscope equipped with bright field optics.

Rice seedling and rice sheath infection assay

Rice seedling infection assays were performed as described with $5x10^4$/ mL conidial

suspension (Kou et al., 2017). Disease symptoms of infection assays were assessed on 7 dpi. The infection assays were repeated three times. For the invasive hyphal development assay, 21-d-old healthy rice seedlings (CO39) were used for sheath preparation. Conidial suspension was inoculated into the rice sheath and incubated in the growth chamber with the photoperiod of 16-h light and 8-h dark at 25°C. The inoculated sheath was trimmed manually and observed by using an Olympus BX53 wide field microscope at 40 hpi.

Yeast two-hybrid analysis

Yeast two-hybrid assays were performed in the yeast strain Y2Hgold with Matchmaker two-hybrid system (Clontech) according to manufacturer's instruction. The baits and preys were cloned to pGADT7 and pGBKT7 respectively. The transformants were grown on the basic medium without tryptophan and leucine at 30°C for about 2 d, and subsequently the direct interaction between two proteins were tested with grown on the selective medium without tryptophan, leucine, histidine and adenine for 4-6 d.

Western blotting analysis

For detecting Flag/GFP-tagged proteins, 0.1 g mycelia cultured in the liquid CM for 2 d were collected. Total protein was extracted with lysis buffer (50 mM Tris-HCl pH 7.4, 150 mM NaCl, 1 mM EDTA, 1% Triton 100 and 1 × protein inhibitor). The resulting protein was separated by 8-15% SDS polyacrylamide gel electrophoresis (SDS-PAGE) and transferred to PVDF membrane, subsequently detected by immunoblotting with anti-Flag (Sigma, A8592) or anti-GFP (Abcam, ab290) antibody.

For detecting histones, the nuclei of 0.5 g mycelia were isolated with extraction buffer (20 mM Tris pH 7.5, 20 mM KCl, 2 mM $MgCl_2$, 25% Glycerol, 250 mM Sucrose, 0.1 mM PMSF, 5 mM beta-mercaptoethanol, 1 × proteinase inhibitors) and filtered through two layers of Miracloth (Millipore). Then the histones were extracted with lysis buffer (50 mM Tris-HCl pH 7.4, 150 mM NaCl, 1 mM EDTA, 1% Triton 100 and 1 × protein inhibitor). Total histones were separated by 15% SDS-PAGE gel and protein blots were detected with anti-H3 (Millipore, 06-755), anti-H3K27me3 (Abcam, ab6002), anti-H3K4me3 (Abcam, ab1012), anti-H3K36me3 (Abcam, ab9050), anti-

H3K4ac (Active motif, 39381), anti-H3K9ac (PTMBIO, PTM-112), anti-H3K18ac (PTMBIO, PTM-158), anti-H3K27ac (Abcam, ab177178) and anti-H4K5ac (Millipore, 07-327) antibody. The relative intensity of Western blots was quantified by Image J software.

Co-immunoprecipitation assays

To perform co-immunoprecipitation assays, 0.5 g mycelia cultured in the liquid CM for 2 d were harvested. Total protein was extracted with lysis buffer (50 mM Tris-HCl pH 7.4, 150 mM NaCl, 1 mM EDTA, 1% Triton 100 and 1 × protein inhibitor) and subsequently precipitated with anti-Flag M2 Magnetic beads (Sigma, M8823) or GFP-Trap (Chromotek, gtma-20) respectively according to the manufacture's instruction. The precipitated protein and input control were detected by the Western blotting with anti-Flag (Sigma, A8592) or anti-GFP (Abcam, ab290) antibody.

mRNA expression analysis with RT-qPCR

Total RNA was extracted from CM cultivated mycelia for 2 d from three biological repeats using the TRIzol (Invitrogen, USA) reagent. Subsequently total RNAs were reversely transcribed into cDNAs with commercial kits (TOYOBO, FSQ-301) according to the manufacturer's instruction. RT-qPCR was performed using SYBR Green qPCR Master Mix (TOYOBO, QST-100) in the LightCycler480 system (Roche). The constitutively expressed *tubulin* gene (*MGG_00604*) was used as endogenous control to normalize amount of cDNA templates. Primers used in the experiments were listed and described in Supplemental Table 2.

RNA-seq analysis

Total RNA was extracted from mycelia from three biological repeats using the TRIzol (Invitrogen, USA) reagent according to the manufacturer's instruction. RNAs were sequenced separately at Novogene, using Illumina Hiseq X-Ten with Hiseq-PE150 strategy. The clean reads were mapped to the reference genome of *M. oryzae* (*M. oryzae* 70-15 assembly MG8 from NCBI) using TopHat software with default settings (Daehwan Kim, 2013). For analysis of differential expression, the assembled transcripts

from three independent biological replicates in the WT and deletion mutants were included and compared using Cuffdiff with default settings (Trapnell et al., 2010). Gene with false discovery rate (FDR) threshold of 0.05 in conjunction with at least 2-fold change in expression level was considered differentially expressed. To calculate the significance of the overlap of two gene sets, P value with Fisher's exact test for overlapping was performed on online (the total number of genes in the *M. oryzae* genome used was 14317) (http://nemates.org/MA/progs/overlap_stats.html). GO analysis for enriched biological processes was perform using DAVID (https://david.ncifcrf.gov/home.jsp) with default settings.

ChIP and ChIP-seq analysis

The ChIP experiments with mycelia were conducted as previous reports with minor modification (He et al., 2018, Tao et al., 2017). Briefly, 1 g mycelia were crosslinked with 1% formaldehyde for 20 mins and stopped with 125 mM glycine for 5 mins at room temperature. Samples were ground with liquid nitrogen and resuspended in the nuclei isolating buffer (10 mM Tris pH 8.0, 10 mM Sodium butyrate, 400 mM Sucrose, 0.1 mM PMSF, 5 mM Beta-Mercaptoethanol, 1 × proteinase inhibitors). Subsequently the precipitated nuclei were used to total chromatin extraction with 1 mL lysis buffer (50 mM HEPES pH7.5, 150 mM NaCl, 1mM EDTA, 10 mM Sodium butyrate, 0.1% deoxycholate, 0.1% SDS, 1% Triton X-100, 1mM PMSF and 1 × Roche protease inhibitor Cocktail). The obtained chromatin was sonicated into DNA fragments between 200-500 bp using Diagenode Bioruptor (high setting, 16 cycles，every cycle with 30 seconds "on" and 30 seconds "off"). 20 μL chromatin solution? was used to input DNA extraction and the remainder was pre-cleared with 10 μL protein A Dynabeads (Thermofisher, 10001D) for 1 h. Then, the chromatin was incubated with anti-H3K27me3 (Abcam, ab6002) or anti- H3K4ac (Active Motif, 39381) overnight at 4°C. Another 20 μL protein A Dynabeads was used to capture protein-DNA mixture and washed for three times. Protein-DNA mixture was reverse-crosslinked, and DNA was recovered with phenol-chloroform extraction. The recovered DNA was used as template for followed ChIP-qPCR and ChIP-seq. Two biological repeats were carried out.

For ChIP-seq assay, the purified DNA was used as library construction with the NEBNext Ultra II DNA Library Prep Kit for Illumina (NEB, E7645L). High-throughput sequencing was carried out using Illumina Hiseq-PE150 by Novogene Corporation (Beijing, China) for Illumina (Langmead et al., 2009). Subsequently the clean read pairs were mapped to the reference genome with Bowtie2 (Version 2.2.8) (Langmead and Salzberg, 2012) and enriched peaks were called by MACS2 (Version 2.1.1) with default parameters (Zhang et al., 2008). The data was imported into the integrative genomics viewer (IGV) for visualization (James T Robinson, 2011). To assign peaks to proximal genes, the distance of 3-kb flanking the peak summit were extracted. To validate ChIP-seq results, ChIP-qPCR assay with two independent repeats was performed. The level of examined fragments was relative to internal reference gene *TUB5* using quantitative real-time PCR. The PCR primers were listed and described in Table S2.

Data availability

The ChIP-seq and RNA-seq datasets generated in this article were deposited in the Gene Expression Omnibus (GEO) under the accession number GSE166690.

Acknowledgments

We thank Dr. Naweed I. Naqvi of the National University of Singapore for helpful suggestions and critically reading manuscript. Thanks to Dr. Zhou Ming of Zhejiang University for help of bioinformatics analysis. Thanks to Dr. Qi Zhenyu of agricultural experimental station of Zhejiang University for controlling the light environment of artificial climate chamber.

Funding

This research was supported in part by the National Natural Science Foundation of China (31970534 to Z.T., 32000103 to Y.K.), the Fundamental Research Funds for the

Central Universities (2019QNA6014 to Z.T.), key R&D project of China National Rice Research Institute, grand number "CNRRI-2020-04", and Open Project Program (20190301 to Z.T.) of State Key Laboratory of Rice Biology. This project was supported by the Chinese Academy of Agricultural Sciences under the "Elite Youth" program, the Agricultural Sciences and Technologies Innovation Program and Hundred-Talent Program of Zhejiang University.

The funders had no role in the design of the study; in the collection, analyses, or interpretation of data; in the writing of the manuscript, or in the decision to publish the results.

Author contributions

Y.K. and Z.T. conceived and designed the experiments; Y.K., J.Q. and Z.W. performed the experiments; H.S., C.L., J.Y., Z.L. and W.X. provided technical assistance and contributed reagents/materials/analysis tools; Y.K. and Z.T. wrote the paper.

Competing interests: The authors declare no conflict of interest.

References

ADAMS, G. E., CHANDRU, A. & COWLEY, S. M. 2018. Co-repressor, co-activator and general transcription factor: the many faces of the Sin3 histone deacetylase (HDAC) complex. *Biochem J,* 475**,** 3921-3932.

BLACKLEDGE, N. P., ROSE, N. R. & KLOSE, R. J. 2015. Targeting Polycomb systems to regulate gene expression: modifications to a complex story. *Nat Rev Mol Cell Biol,* 16**,** 643-649.

CAVALLI, G. & HEARD, E. 2019. Advances in epigenetics link genetics to the environment and disease. *Nature,* 571**,** 489-499.

CHADHA, S. & SHARMA, M. 2014. Transposable elements as stress adaptive capacitors induce genomic instability in fungal pathogen *Magnaporthe oryzae*. *PLoS One,* 9**,** e94415.

CHUJO, T. & SCOTT, B. 2014. Histone H3K9 and H3K27 methylation regulates fungal alkaloid biosynthesis in a fungal endophyte-plant symbiosis. *Mol Microbiol,* 92**,** 413-34.

CONNOLLY, L. R., SMITH, K. M. & FREITAG, M. 2013. The Fusarium H3K27me3 KMT6 regulates development and expression of secondary metabolite gene clusters. *PLoS Genet,* 9**,** e1003916.

DAEHWAN KIM, G. P., COLE TRAPNELL, HAROLD PIMENTEL, RYAN KELLEY AND STEVEN L SALZBERG 2013.

711 TopHat2: accurate alignment of transcriptomes in the presence of insertions, deletions and
712 gene fusions. *Genome Biol,* 14**,** R36.
713 DING, S. L., LIU, W., ILIUK, A., RIBOT, C., VALLET, J., TAO, A., WANG, Y., LEBRUN, M. H. & XU, J. R. 2010.
714 The Tig1 histone deacetylase complex regulates infectious growth in the rice blast fungus
715 *Magnaporthe oryzae*. *Plant Cell,* 22**,** 2495-508.
716 DONG, Y., LI, Y., QI, Z., ZHENG, X. & ZHANG, Z. 2016. Genome plasticity in filamentous plant pathogens
717 contributes to the emergence of novel effectors and their cellular processes in the host. *Curr*
718 *Genet,* 62**,** 47-51.
719 DONG, Y., LI, Y., ZHAO, M., JING, M., LIU, X., LIU, M., GUO, X., ZHANG, X., CHEN, Y., LIU, Y., LIU, Y., YE, W.,
720 ZHANG, H., WANG, Y., ZHENG, X., WANG, P. & ZHANG, Z. 2015. Global genome and
721 transcriptome analyses of *Magnaporthe oryzae* epidemic isolate 98-06 uncover novel effectors
722 and pathogenicity-related genes, revealing gene gain and lose dynamics in genome evolution.
723 *PLoS Pathog,* 11**,** e1004801.
724 DUMESIC, P. A., HOMER, C. M., MORESCO, J. J., PACK, L. R., SHANLE, E. K., COYLE, S. M., STRAHL, B. D.,
725 FUJIMORI, D. G., YATES, J. R., 3RD & MADHANI, H. D. 2015. Product binding enforces the
726 genomic specificity of a yeast polycomb repressive complex. *Cell,* 160**,** 204-18.
727 FOUCHE, S., PLISSONNEAU, C. & CROLL, D. 2018. The birth and death of effectors in rapidly evolving
728 filamentous pathogen genomes. *Curr Opin Microbiol,* 46**,** 34-42.
729 GRZENDA, A., LOMBERK, G., ZHANG, J. S. & URRUTIA, R. 2009. Sin3: master scaffold and transcriptional
730 corepressor. *Biochim Biophys Acta,* 1789**,** 443-50.
731 GU, X., JIANG, D., YANG, W., JACOB, Y., MICHAELS, S. D. & HE, Y. 2011. *Arabidopsis* homologs of
732 retinoblastoma-associated protein 46/48 associate with a histone deacetylase to act
733 redundantly in chromatin silencing. *PLoS Genet,* 7**,** e1002366.
734 HE, M., XU, Y., CHEN, J., LUO, Y., LV, Y., SU, J., KERSHAW, M. J., LI, W., WANG, J., YIN, J., ZHU, X., LIU, X.,
735 CHERN, M., MA, B., WANG, J., QIN, P., CHEN, W., WANG, Y., WANG, W., REN, Z., WU, X., LI, P.,
736 LI, S., PENG, Y., LIN, F., TALBOT, N. J. & CHEN, X. 2018. MoSnt2-dependent deacetylation of
737 histone H3 mediates MoTor-dependent autophagy and plant infection by the rice blast fungus
738 *Magnaporthe oryzae*. *Autophagy,* 14**,** 1543-1561.
739 HUANG, F., YUAN, W., TIAN, S., ZHENG, Q. & HE, Y. 2019. *SIN3 LIKE* genes mediate long-day induction of
740 flowering but inhibit the floral transition in short days through histone deacetylation in
741 *Arabidopsis*. *Plant J,* 100**,** 101-113.
742 JAMES T ROBINSON, H. T., WENDY WINCKLER, MITCHELL GUTTMAN, ERIC S LANDER, GAD GETZ & JILL
743 P MESIROV 2011. Integrative genomics viewer. *Nature,* 29**,** 24-26.
744 JAMIESON, K., ROUNTREE, M. R., LEWIS, Z. A., STAJICH, J. E. & SELKER, E. U. 2013. Regional control of
745 histone H3 lysine 27 methylation in *Neurospora*. *Proc Natl Acad Sci U S A,* 110**,** 6027-32.
746 JEON, J., LEE, G. W., KIM, K. T., PARK, S. Y., KIM, S., KWON, S., HUH, A., CHUNG, H., LEE, D. Y., KIM, C. Y. &
747 LEE, Y. H. 2020. Transcriptome profiling of the rice blast fungus *Magnaporthe oryzae* and its
748 host *Oryza sativa* during infection. *Mol Plant Microbe Interact,* 33**,** 141-144.
749 JULIA I. QüESTA, J. S., NUNO GERALDO, HAILONG AN, CAROLINE DEAN 2016. *Arabidopsis* transcriptional
750 repressor VAL1 triggers Polycomb silencing at *FLC* during vernalization. 353**,** 485-488.
751 KASSIS, J. A. & BROWN, J. L. 2013. Polycomb group response elements in *Drosophila* and vertebrates.
752 *Adv Genet,* 81**,** 83-118.
753 KHANG, C. H., BERRUYER, R., GIRALDO, M. C., KANKANALA, P., PARK, S. Y., CZYMMEK, K., KANG, S. &
754 VALENT, B. 2010. Translocation of Magnaporthe oryzae effectors into rice cells and their

subsequent cell-to-cell movement. *Plant Cell,* 22**,** 1388-403.

KOU, Y., TAN, Y. H., RAMANUJAM, R. & NAQVI, N. I. 2017. Structure-function analyses of the Pth11 receptor reveal an important role for CFEM motif and redox regulation in rice blast. *New Phytol,* 214**,** 330-342.

LANGMEAD, B. & SALZBERG, S. L. 2012. Fast gapped-read alignment with Bowtie 2. *Nat Methods,* 9**,** 357-9.

LANGMEAD, B., TRAPNELL, C., POP, M. & SALZBERG, S. L. 2009. Ultrafast and memory-efficient alignment of short DNA sequences to the human genome. *Genome Biol,* 10**,** R25.

LANZUOLO, C. & ORLANDO, V. 2012. Memories from the polycomb group proteins. *Annu Rev Genet,* 46**,** 561-89.

LEE, J., LEE, J. J. & JEON, J. 2019. A histone deacetylase, MoHOS2 regulates asexual development and virulence in the rice blast fungus. *J Microbiol,* 57**,** 1115-1125.

LUO, X. & HE, Y. 2020. Experiencing winter for spring flowering: A molecular epigenetic perspective on vernalization. *J Integr Plant Biol,* 62**,** 104-117.

MARGUERON, R. & REINBERG, D. 2011. The Polycomb complex PRC2 and its mark in life. *Nature,* 469**,** 343-9.

MEHDI, S., DERKACHEVA, M., RAMSTROM, M., KRALEMANN, L., BERGQUIST, J. & HENNIG, L. 2016. The WD40 domain protein MSI1 functions in a histone deacetylase complex to fine-tune abscisic acid signaling. *Plant Cell,* 28**,** 42-54.

MOSQUERA, G., GIRALDO, M. C., KHANG, C. H., COUGHLAN, S. & VALENT, B. 2009. Interaction transcriptome analysis identifies *Magnaporthe oryzae* BAS1-4 as Biotrophy-associated secreted proteins in rice blast disease. *Plant Cell,* 21**,** 1273-90.

NETEA, M. G., JOOSTEN, L. A., LATZ, E., MILLS, K. H., NATOLI, G., STUNNENBERG, H. G., O'NEILL, L. A. & XAVIER, R. J. 2016. Trained immunity: A program of innate immune memory in health and disease. *Science,* 352**,** aaf1098.

PHAM, K. T., INOUE, Y., VU, B. V., NGUYEN, H. H., NAKAYASHIKI, T., IKEDA, K. & NAKAYASHIKI, H. 2015. MoSET1 (histone H3K4 methyltransferase in *Magnaporthe oryzae*) regulates global gene expression during infection-related morphogenesis. *PLoS Genet,* 11**,** e1005385.

RIDENOUR, J. B., MOLLER, M. & FREITAG, M. 2020. Polycomb repression without bristles: facultative heterochromatin and genome stability in fungi. *Genes (Basel),* 11**,** 638.

SANCHEZ-VALLET, A., FOUCHE, S., FUDAL, I., HARTMANN, F. E., SOYER, J. L., TELLIER, A. & CROLL, D. 2018. The genome biology of effector gene evolution in filamentous plant pathogens. *Annu Rev Phytopathol,* 56**,** 21-40.

SCHUETTENGRUBER, B., BOURBON, H. M., DI CROCE, L. & CAVALLI, G. 2017. Genome regulation by Polycomb and Trithorax: 70 years and counting. *Cell,* 171**,** 34-57.

SHARPEE, W., OH, Y., YI, M., FRANCK, W., EYRE, A., OKAGAKI, L. H., VALENT, B. & DEAN, R. A. 2017. Identification and characterization of suppressors of plant cell death (SPD) effectors from *Magnaporthe oryzae*. *Mol Plant Pathol,* 18**,** 850-863.

TAO, Z., SHEN, L., GU, X., WANG, Y., YU, H. & HE, Y. 2017. Embryonic epigenetic reprogramming by a pioneer transcription factor in plants. *Nature,* 551**,** 124-128.

TRAPNELL, C., WILLIAMS, B. A., PERTEA, G., MORTAZAVI, A., KWAN, G., VAN BAREN, M. J., SALZBERG, S. L., WOLD, B. J. & PACHTER, L. 2010. Transcript assembly and quantification by RNA-Seq reveals unannotated transcripts and isoform switching during cell differentiation. *Nat Biotechnol,* 28**,** 511-5.

WANG, L., CHEN, H., LI, J., SHU, H., ZHANG, X., WANG, Y., TYLER, B. M. & DONG, S. 2020. Effector gene silencing mediated by histone methylation underpins host adaptation in an *oomycete* plant pathogen. *Nucleic Acids Res,* 48**,** 1790-1799.

WILES, E. T. & SELKER, E. U. 2017. H3K27 methylation: a promiscuous repressive chromatin mark. *Curr Opin Genet Dev,* 43**,** 31-37.

XIAO, J., JIN, R., YU, X., SHEN, M., WAGNER, J. D., PAI, A., SONG, C., ZHUANG, M., KLASFELD, S., HE, C., SANTOS, A. M., HELLIWELL, C., PRUNEDA-PAZ, J. L., KAY, S. A., LIN, X., CUI, S., GARCIA, M. F., CLARENZ, O., GOODRICH, J., ZHANG, X., AUSTIN, R. S., BONASIO, R. & WAGNER, D. 2017. *Cis* and *trans* determinants of epigenetic silencing by Polycomb repressive complex 2 in Arabidopsis. *Nat Genet,* 49**,** 1546-1552.

ZHANG, S., LIANG, M., NAQVI, N. I., LIN, C., QIAN, W., ZHANG, L. H. & DENG, Y. Z. 2017. Phototrophy and starvation-based induction of autophagy upon removal of Gcn5-catalyzed acetylation of Atg7 in *Magnaporthe oryzae*. *Autophagy,* 13**,** 1318-1330.

ZHANG, W., HUANG, J. & COOK, D. E. 2021. Histone modification dynamics at H3K27 are associated with altered transcription of *in planta* induced genes in *Magnaporthe oryzae*. *PLoS Genet,* 17**,** e1009376.

ZHANG, Y., LIU, T., MEYER, C. A., EECKHOUTE, J., JOHNSON, D. S., BERNSTEIN, B. E., NUSBAUM, C., MYERS, R. M., BROWN, M., LI, W. & LIU, X. S. 2008. Model-based analysis of ChIP-Seq (MACS). *Genome Biol,* 9**,** R137.

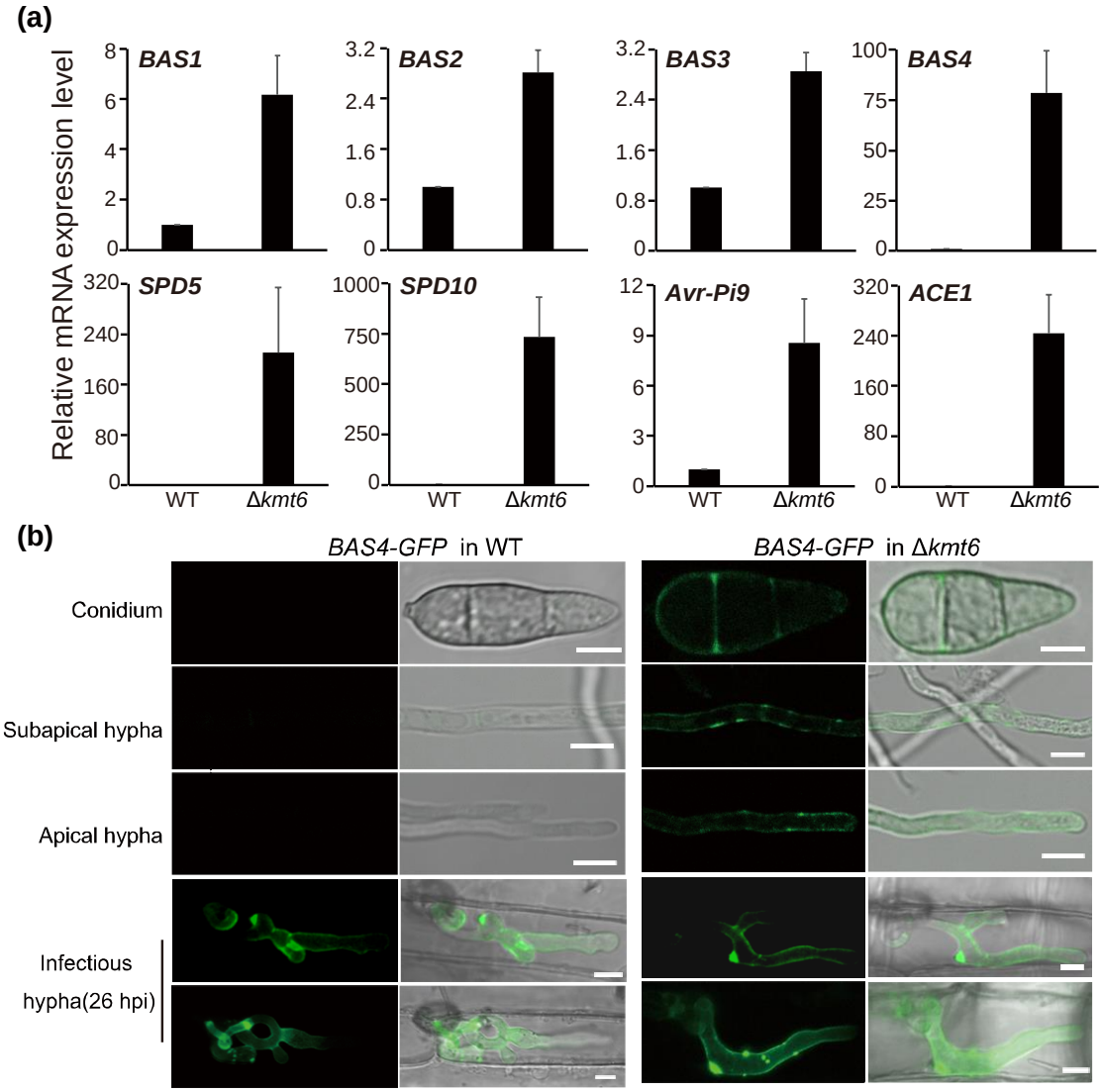

Figure 1. Loss of *KMT6* results in activation of *effectors* in the vegetative growth stage in *M. oryzae*. (a) Relative expression level of representative *effectors* in the WT and Δ*kmt6* strains by qRT-PCR. The *β-tubulin* gene was used as the endogenous reference gene. Bar means standard error of three biological repeats. (b) Confocal microscopy image of Bas4-GFP in the vegetative and *in planta* growth stages of the WT and Δ*kmt6* strains. In the WT, Bas4-GFP fluorescence is only presented in the *in planta* growth stage, while in the Δ*kmt6*, Bas4-GFP fluorescence could be detected in the conidia, apical hypha, subapical hypha and invasive hypha. Bar = 5 μm.

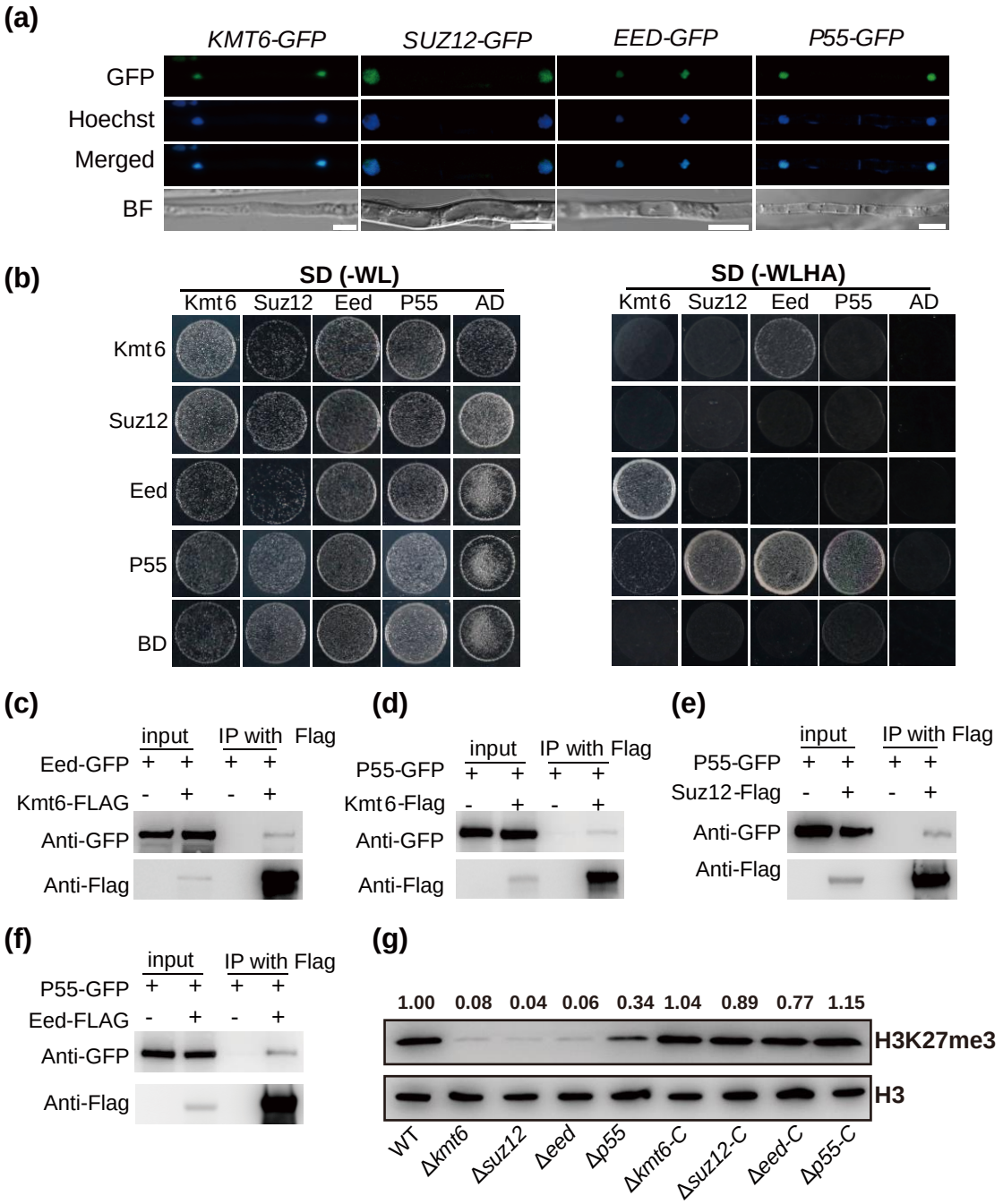

Figure 2. Core subunits Kmt6, Eed, Suz12, together with P55, are involved in the Poly-comb repressive complex 2 in *M. oryzae*.

(a) Confocal microscopy-based subcellular localization of PRC2 subunits fused with GFP. The GFP signal co-localized with Hoechst (10 μg/mL) stained nuclei. Bar = 5 μm. (b) Yeast-two-hybrid assay of PRC2 components Kmt6, Eed, Suz12 and P55. The bait and prey plasmids were co-transformed into yeast strain Y2Hgold respectively, then the transformants were grown on basal medium SD (-WL, without tryptophan and leucine) and selective medium SD (-WLHA, without tryptophan, leucine, histidine and adenine). (c-f) Co-immuoprecipitation (CoIP) was performed with the strains expressing both *Kmt6-Flag* and *Suz12-GFP*, *P55-GFP* and *Kmt6-Flag*, *P55-GFP* and *Suz12-Flag*, or *P55-GFP* and *Eed-Flag*. (g) Western blot detection of histone H3 and histone

methylation H3K27me3 in the WT, Δ*kmt6*, Δ*eed*, Δ*suz12* and Δ*P55* strains. The intensity abundance was measured and calculated relative to that of the WT. Two repeated biological experiments were carried out and the results were similar.

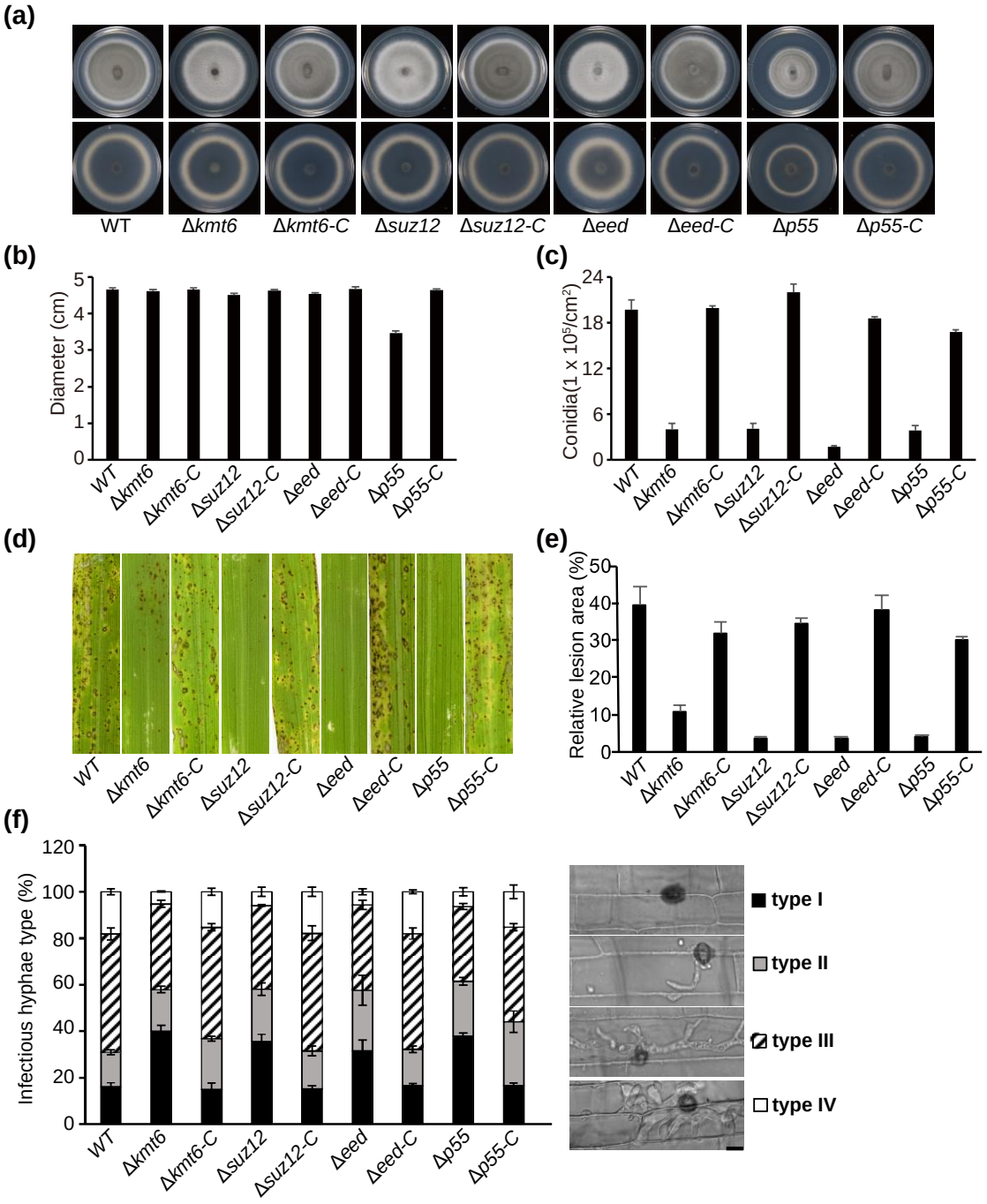

Figure 3. PRC2 complex is required for fungal growth and pathogenicity in *M. oryzae*.

(a) Radical growth of the WT, Δ*kmt6*, Δ*eed*, Δ*suz12*, Δ*P55* and their complementation strains. Colonies of indicated strains were grown on the PA medium for 7 d, then both up and bottom sides of colonies were imaged. (b) Statistical analysis of colonies diameters of tested strains on the PA medium. (c) Bar charts showing the conidia that produced in the indicated strain of *M. oryzae*. (d) Observation and statistical analysis of invasive hypha growth in rice sheath cells at 40 hpi. Four types of invasive hypha (illustrated in the right panel with corresponding column): no penetration, penetration with primary hyphae, with differentiated secondary invasive hyphae, and invasive hyphae spreading into neighbouring cells, were quantified. Data represents mean ± SD

of three independent repeats, with n = 300 appressoria per analysis. Scale bar = 5 μm. (e) Blast infection assays using rice seedlings (*Oryza sativa* L., cultivar CO39). Deletion of *KMT6*, *EED*, *SUZ12* and *P55* impaired the pathogenicity of *M. oryzae*. (f) Relative lesions area of indicated strains. The relative area of lesions was quantified by Image J software. Data represents the mean ± SD from three independent replicates.

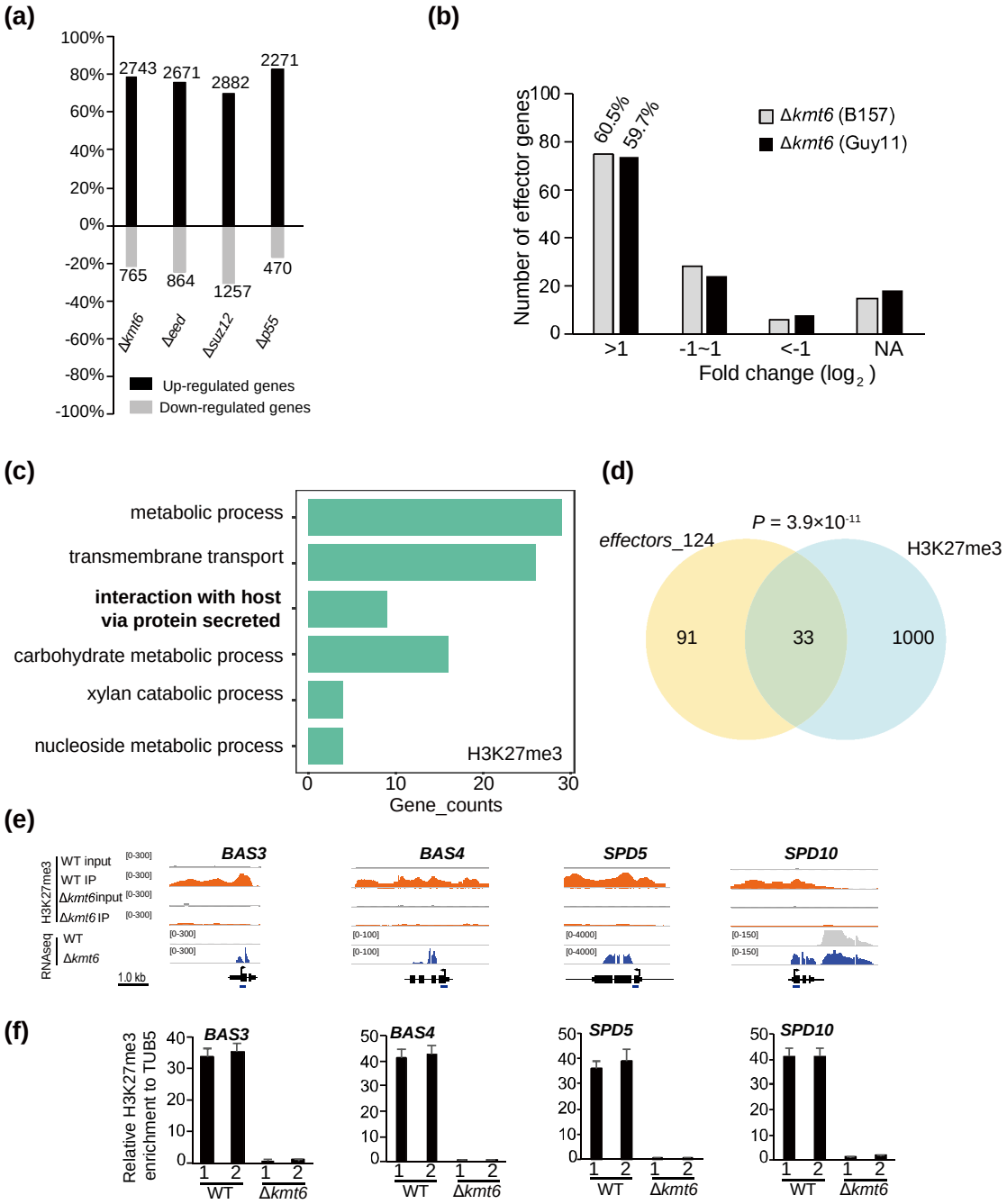

Figure 4. PRC2-mediated H3K27me3 activity is necessary for the suppression of *effectors* during vegetative growth stage in *M. oryzae*.

(a) Summary of up- and down-regulated genes in the different *PRC2* component mutants with RNA-seq analysis. The number at the top or bottom is the number of DEGs in the mutant. The Y-axis is the percentage of up- and down-regulated genes in all DEGs. Data was obtained from three independent biological repeats. (b) The distribution of 124 *effectors* based on the expression change in Δ*kmt6*-UEG (B157) and Δ*kmt6*-UEG (Guy11) compared with that of their WT respectively with our RNA-seq analysis. (c) GO analysis of H3K27me3 marked genes. (d) The Venn diagram showing statistically significant overlap between gene sets of H3K27me3 marked genes and putative 124 *effectors*. (e) Genome browser views of H3K27me3 occupancy from

ChIP-seq and expression pattern from RNA-seq of selected genes. ChIP-seq was conducted with two biological repeats. The number areas were reads per million (RPM). (f) ChIP-qPCR verified the enrichment of H3K27me3 at the chromatin of selected *effectors*. The examined regions were shown at the bottom. The relative enrichments were calculated by relative quantitation from two biological repeats, which was standardized with internal control *TUB5*, and then compared with that of WT. Bar represents standard error from three technical repeats.

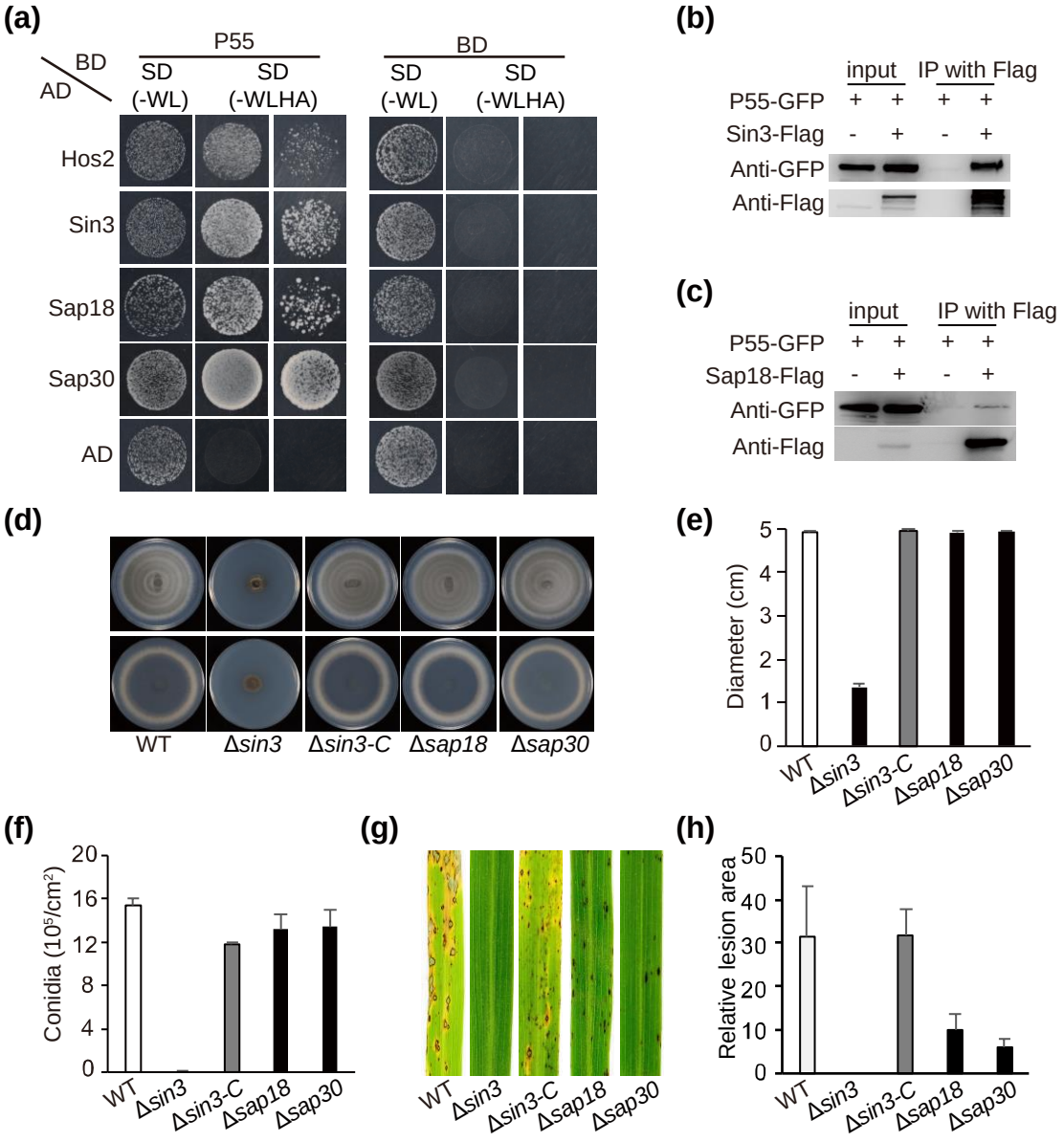

Figure 5. P55 associates with Sin3-HDAC complex which is required for pathogenicity in *M. oryzae*.

(a) Yeast-two-hybrid assay of P55 and Sin3-HDAC component HDAC, Sin3, Sap18, and Sap30. The bait and prey plasmids were co-transformed into yeast strain Y2Hgold respectively, then the transformants were grown on basal medium SD (-WL) and selective medium SD (-WLHA). (b-c) Co-immunoprecipitation assays were performed with the strains expressing Sin3-Flag and P55-GFP**,** Sap18-Flag and P55-GFP. (d-e) Radical growth of the *SIN3-HDAC* deletion strains on the PA medium cultured for 7 d. (f) Deletion of *Sin3* resulted in decreased conidiation. (g-h) *Sin3-HDAC* is required for pathogenicity of *M. oryzae*. Rice seedling infection assay of the WT and *Sin3-HDAC* deletion strains with cultivar Co39. Similar results were obtained from two biological repeats.

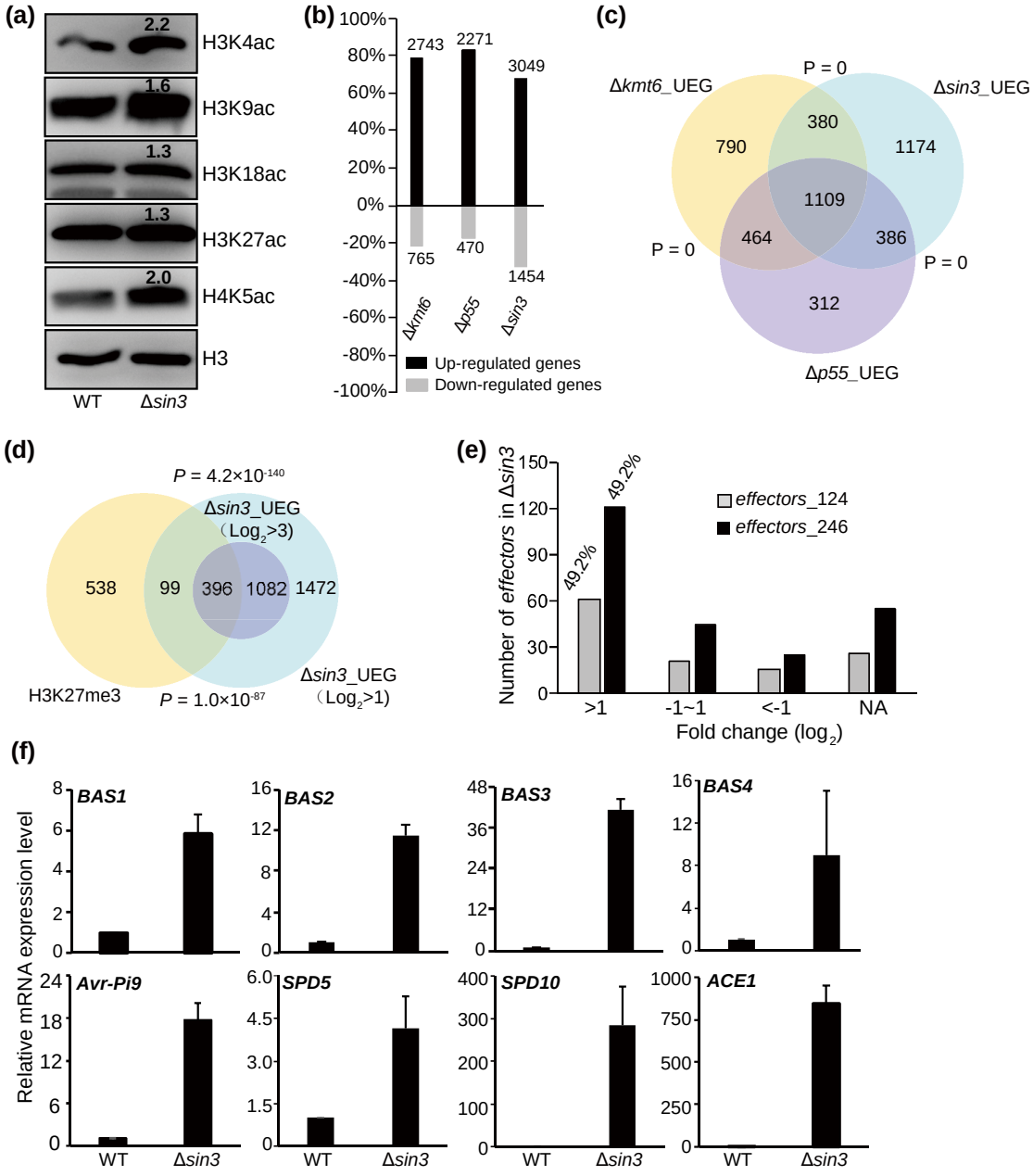

Figure 6. Sin3-HDAC coordinates with PRC2 to prompt H3K27me3-mediated transcriptional silencing on *effectors*.

(a) Levels of histone acetylation at the examined residues were measured by Western blotting assay in the WT and Δ*sin3* strains. The number at the top of band is the relative intensity calculated by Image J software. Similar results were obtained from three biological repeats. (b) Summary of up- and down-regulated genes in the Δ*p55* and Δ*sin3* by comparing with that of WT. The number at the top or bottom is the number of DEG in the mutant. The Y-axis is the percentage of up- and down-regulated genes in all DEG. Data was obtained from three biological repeats. (c) The Venn diagram showing statistically significant overlaps among genes sets of Δ*sin3*-UEG, Δ*p55*-UEG and Δ*kmt6*-UEG. P value with Fisher's exact test for overlapping between gene sets were labeled. (d) The Venn diagram showing statistically significant overlap between genes

sets of H3K27me3-marked genes and Δ*sin3*-UEG. (e) The distribution of putative 124 and 246 *effectors* based on the expression change in Δ*sin3*-UEG. (f) Relative expression level of representative *effectors* were checked in WT and Δ*sin3* by qRT-PCR. Data represents mean±SD of three independent biological replicates.

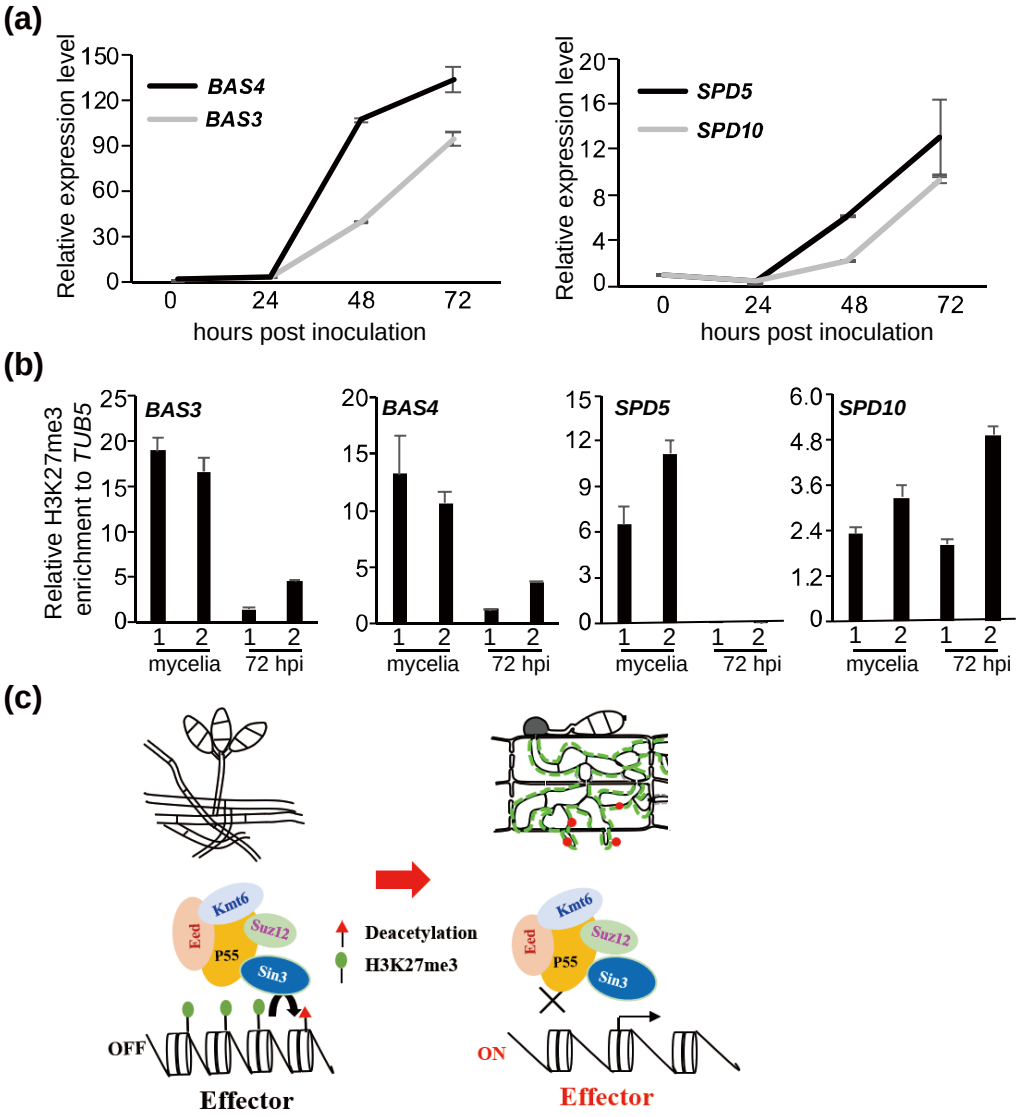

Figure 7. H3K27me3 modification is "erased" from the chromatin of *effectors* at the early stage of infection.

(a) The expression of the *effectors BAS3*, *BAS4*, *SPD5*, and *SPD10* were induced by host.

(b) H3K27me3 modification at the chromatin of *effectors* was removed at the early stage of infection.

(c) Model of *effectors* reprogramming during transition from vegetative growth to *in planta* growth. During vegetative growth stage, PRC2 coordinates with Sin3 histone deacetylase complex suppresses the expression of *effectors* in *M. oryzae*, while during the invasion growth stage, H3K27me3 modification is "erased" upon the perception of signals from host, then the *effectors* are expressed.

Supporting Information

Article title: Suppression of histone modification epigenetically reprograms the genome-wide expression of *effectors* during *Magnaporthe oryzae*–rice interaction

The following Supporting Information is available for this article:

Figure S1. Phylogenetic analysis of PRC2 components in *M. oryzae*.

Figure S2. Detection of H3K4me3 and H3K36me3 level in the deletion strains by Western blot analysis.

Figure S3. Bioinformatics analysis of PRC2 subunits based on RNA-seq.

Figure S4. Expression pattern of *effectors* in the *PRC2* mutants.

Figure S5. Expression pattern of *effectors* in the Δ*kmt6*(Guy11) mutant.

Figure S6. Absence of H3K27me3 partially mimics host-derived signal.

Figure S7. H3K27me3 modification deposits on the chromatin of *effectors* and infection-specific genes during vegetative growth stage.

Figure S8. Sin3 histone deacetylase complex contributes to histone deacetylation.

Figure S9. GO analysis on gene sets of Δ*sin3*-UEG.

Figure S10. Confocal microscopy-based subcellular localization of Bas4-GFP in the vegetative and *in planta* growth stages in the WT and Δ*sin3* strains.

Table S1. Components of polycomb repressive complex in *M. oryzae*, *N. crassa*, *A. thaliana*, and *D. melanogaster*.

Table S2. Primers used in this study.

Table S3. Strains used in this study.

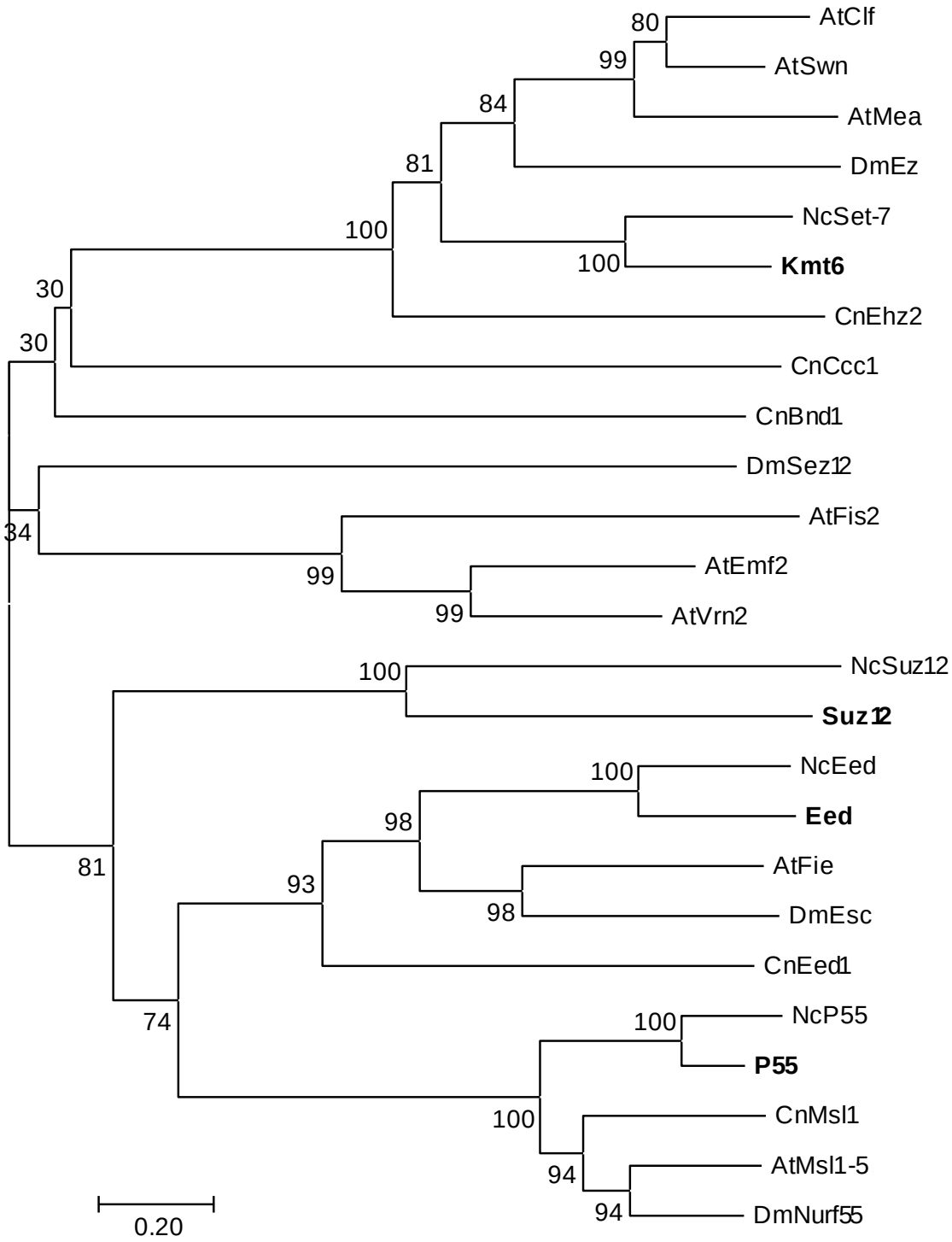

Figure S1. Phylogenetic analysis of PRC2 components in *M. oryzae*. The phylogenetic tree of PRC2 components from *M. oryzae* (highlighted with bold font), *N. crassa*, *A. thaliana*, and *D. melanogaster* was constructed by CLUSTAL_W and MEGA 7 programs using neighbor-joining method with 1000 bootstrap replicates. Genbank accession numbers of these protein were listed in S1 Table.

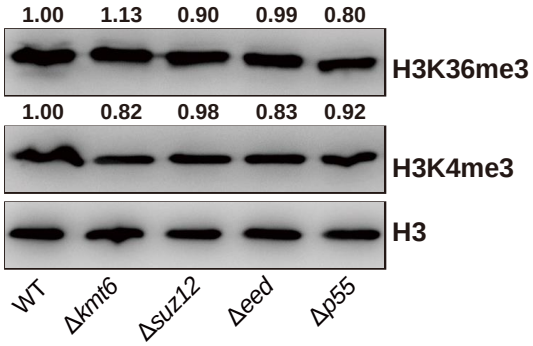

Figure S2. Detection of H3K4me3 and H3K36me3 level in the deletion strains by Western blot analysis.

The number at the top of band was the relative intensity calculated with Image J software. Two biological replicates were carried out with similar results.

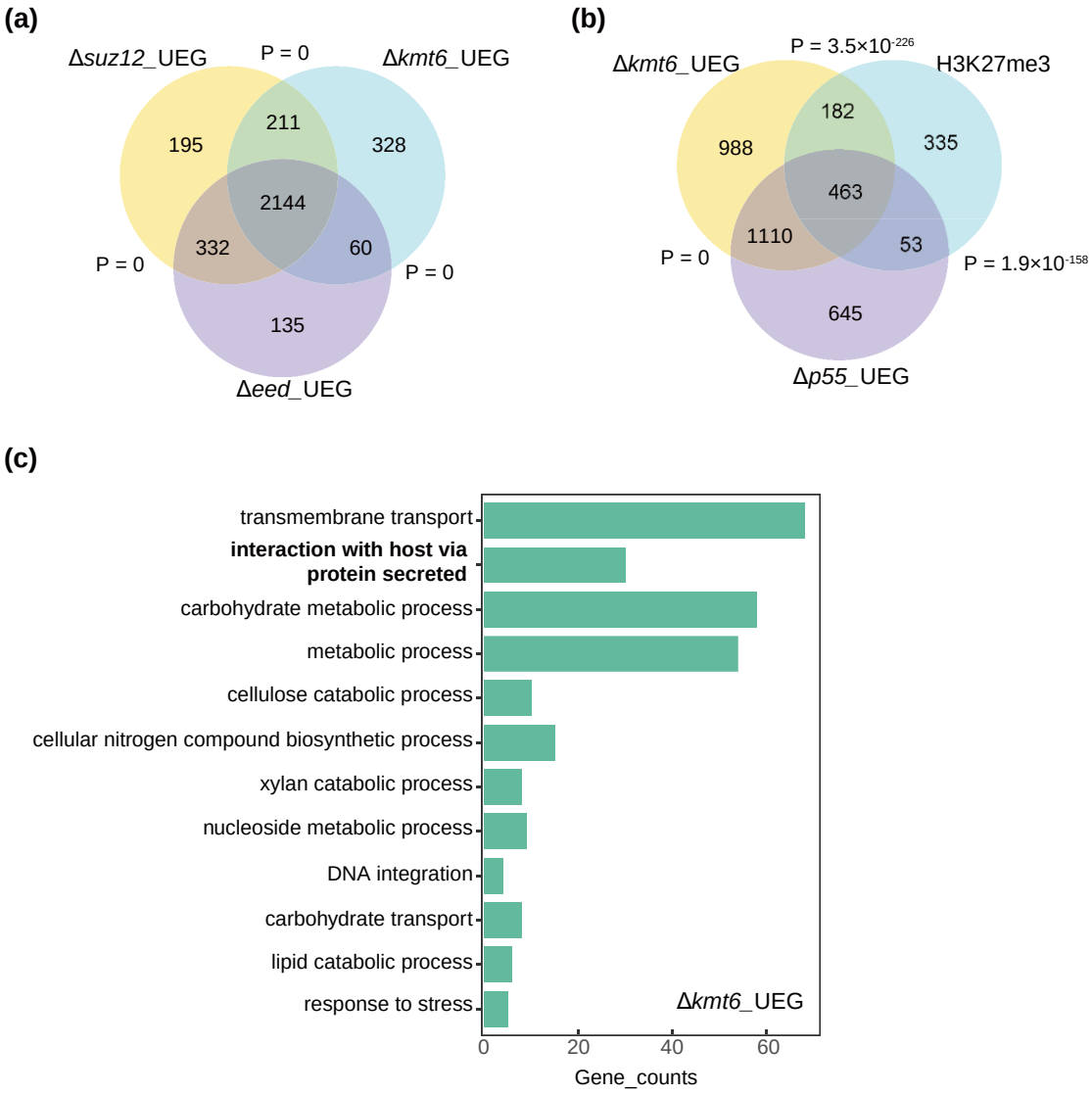

Figure S3. Bioinformatics analysis of PRC2 subunits based on RNA-seq.

(a) The Venn diagram showing statistically significant overlaps among genes sets of the Δ*kmt6*-UEG, Δ*suz12*-UEG and Δ*eed*-UEG. P value for overlapping between gene sets was obtained by Fisher's exact test.
(b) The Venn diagram showing significant overlap among gene sets of Δ*kmt6*-UEG, Δ*p55*-UEG and H3K27me3 marked genes.
(c) GO analysis on gene sets of the Δ*kmt6*-UEG.

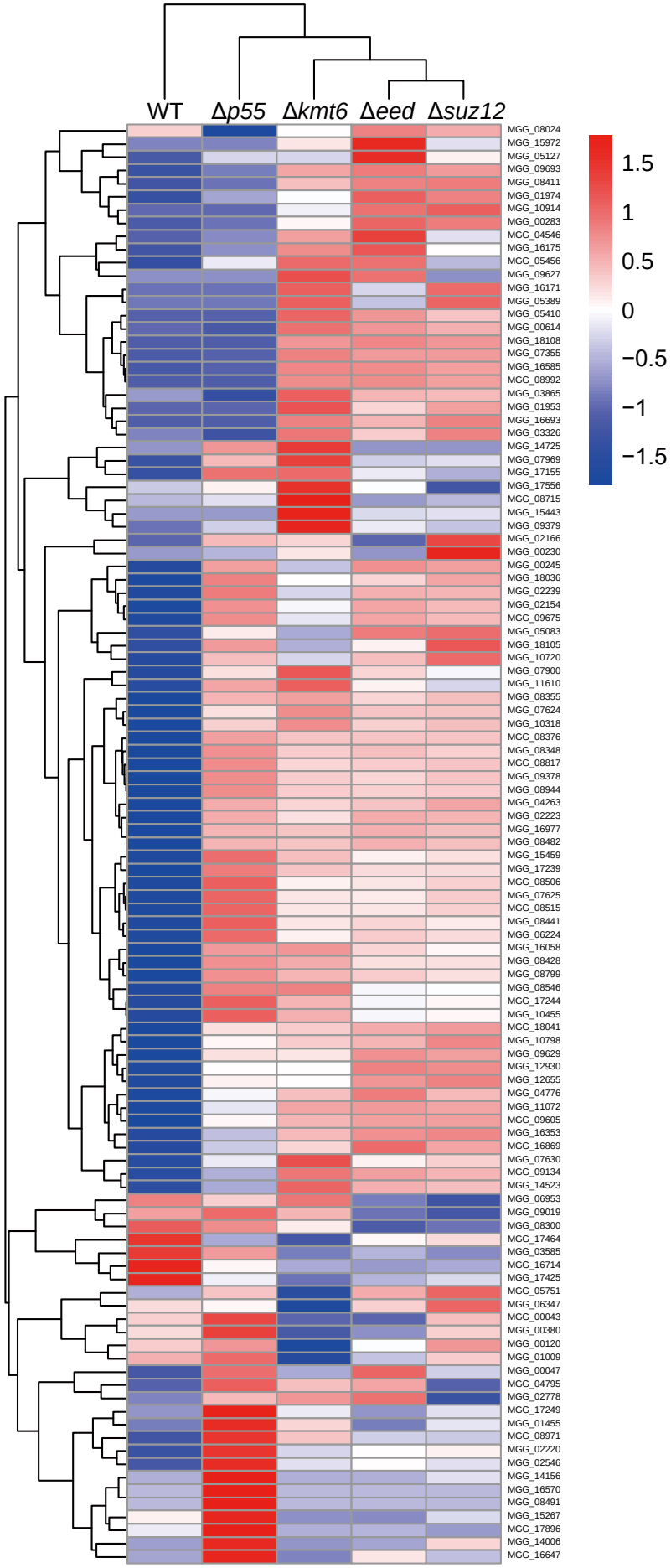

Figure S4. **Expression pattern of *effectors* in the *PRC2* mutants.**

Heat maps illustrated expression changes of genome-wide e*ffectors* in different *PRC2* mutant compared with that of WT B157. Three biological replications of RNA-Seq sequencing were conducted on independent samples.

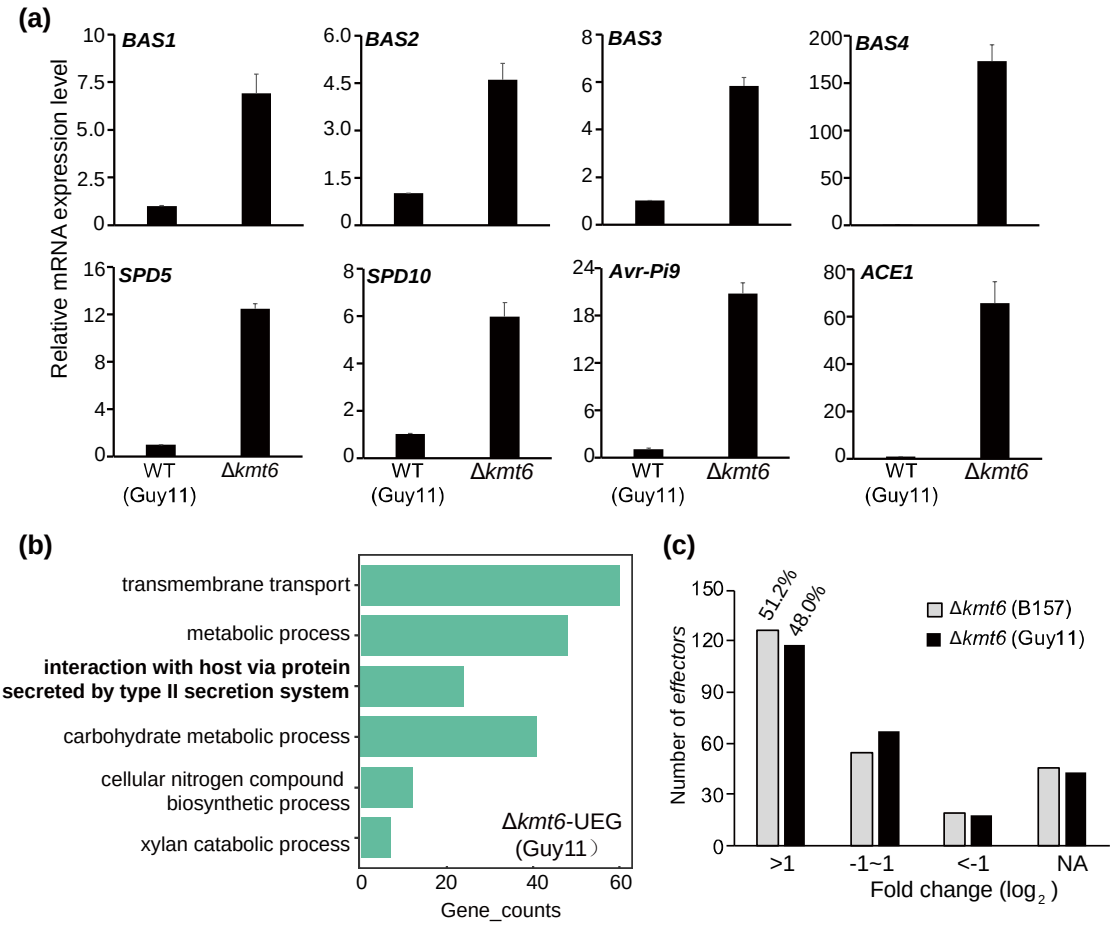

Figure S5. Expression pattern of *effectors* in the Δ*kmt6*(Guy11) mutant.

(a) Relative expression level of representative *effectors* in Guy11 and Δ*kmt6*(Guy11). Values are means ± SD of three biological replicates.

(b) GO analysis on gene sets of the Δ*kmt6*-UEG (Guy11).

(c) The distribution of putative 246 *effectors* based on the expression level change in the Δ*kmt6*-UEG (B157) and Δ*kmt6*-UEG (Guy11).

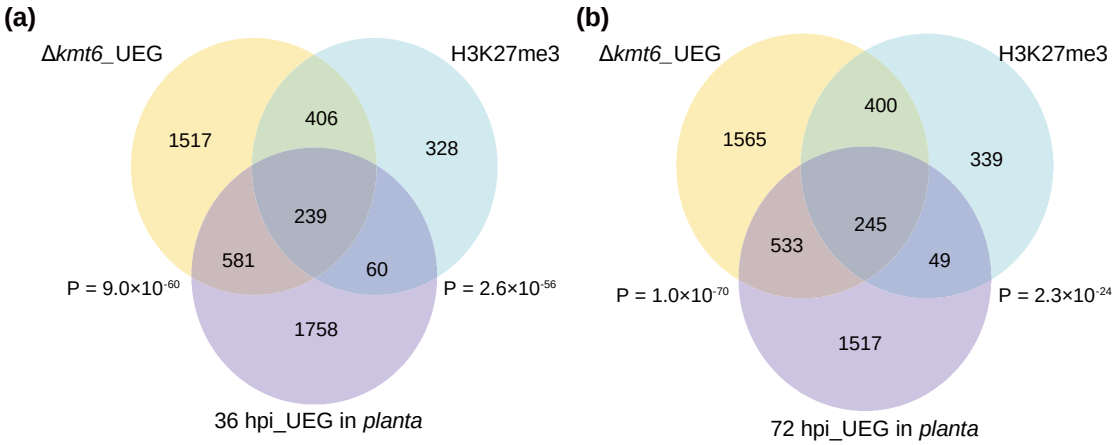

Figure S6. Absence of H3K27me3 partially mimics host-derived signal.
(a) The Venn diagram shows statistically significant overlaps among genes sets of the Δ*kmt6*-UEG, 36 hpi_UEG *in planta* and H3K27me3 marked genes.
(b) The Venn diagram represents statistically significant overlaps among genes sets of Δ*kmt6*-UEG, 72 hpi_UEG *in planta* and H3K27me3 marked genes.

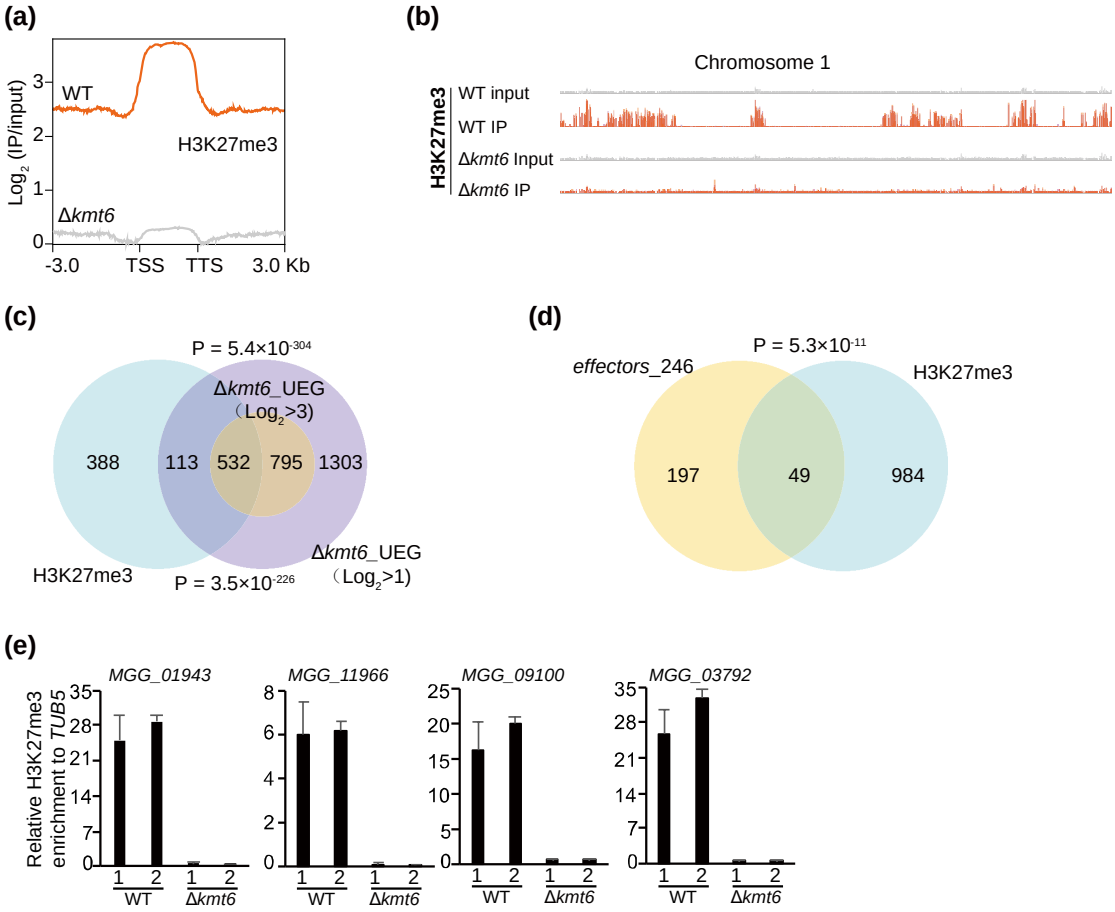

Figure S7. H3K27me3 modification deposits on the chromatin of *effectors* and infection-specific genes during vegetative growth stage.

(a) The average H3K27me3 occupancy within 3 Kb genomic regions flanking the summit of H3K27me3 peaks in the WT and Δ*kmt6* strains.

(b) Genome browser views of H3K27me3 occupancy on the chromosome 1 in the WT and Δ*kmt6* strains.

(c) The Venn diagram shows statistically significant overlaps between gene sets of H3K27me3 marked genes and the Δ*kmt6*_UEG with threshold of $Log_2 > 1$ and $Log_2 > 3$ respectively. P value with Fisher's exact test for overlapping between gene sets were labeled.

(d) The Venn diagram shows significant overlap among gene sets of putative 246 *effectors* and H3K27me3 marked genes.

(e) ChIP-qPCR verified the enrichment of H3K27me3 on the chromatin of infection-specific genes. The relative enrichments were calculated by relative quantitation of two biological repeats, which was standardized by internal control *TUB5*, and then compared with that of WT. Bar represents standard error from three technical repeats.

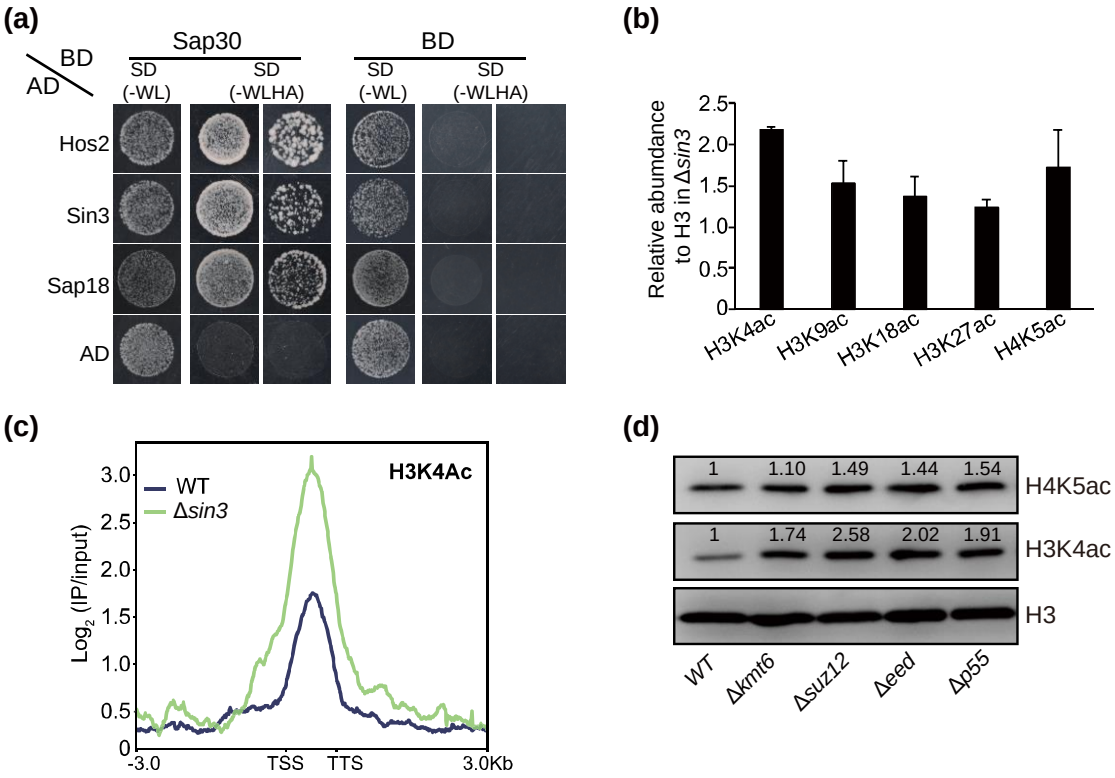

Figure S8. Sin3 histone deacetylase complex contributes to histone deacetylation.

(a) Yeast-two-hybrid assay of interaction between Sap30 and other Sin3-HDAC components Hos2, Sin3, or Sap18. The bait and prey plasmids were co-transformed into yeast strain Y2Hgold respectively, then the transformants were grown on basal medium SD (-WL) and selective medium SD (-WLHA).

(b) Relative abundance of examined protein blots in the WT and Δ*sin3* strains. The standard error was obtained from three biological repetitions.

(c) Bolt representation of the average H3K4ac occupancy within 3 Kb genomic regions flanking the summit of H3K4ac peaks in the WT and Δ*sin3* mutant.

(d) Western blotting assay detected the H4K5ac and H3K4ac modification in the deletion strains of PRC2 subunits. The number at the top of band was the relative intensity calculated with Image J. Two biological replicates were carried out with similar results.

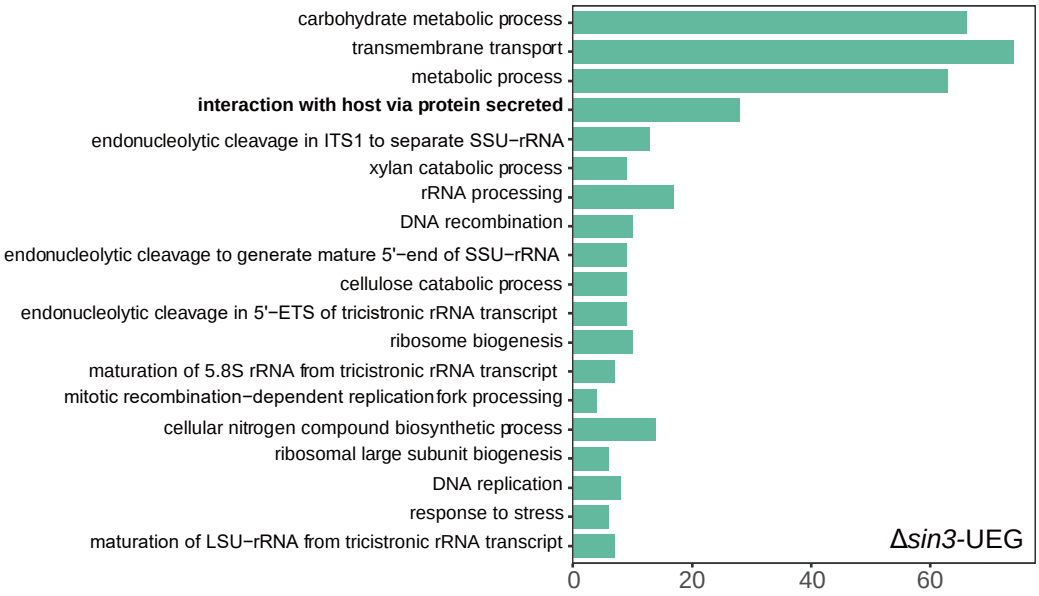

Figure S9. GO analysis on gene sets of Δ*sin3*-UEG.

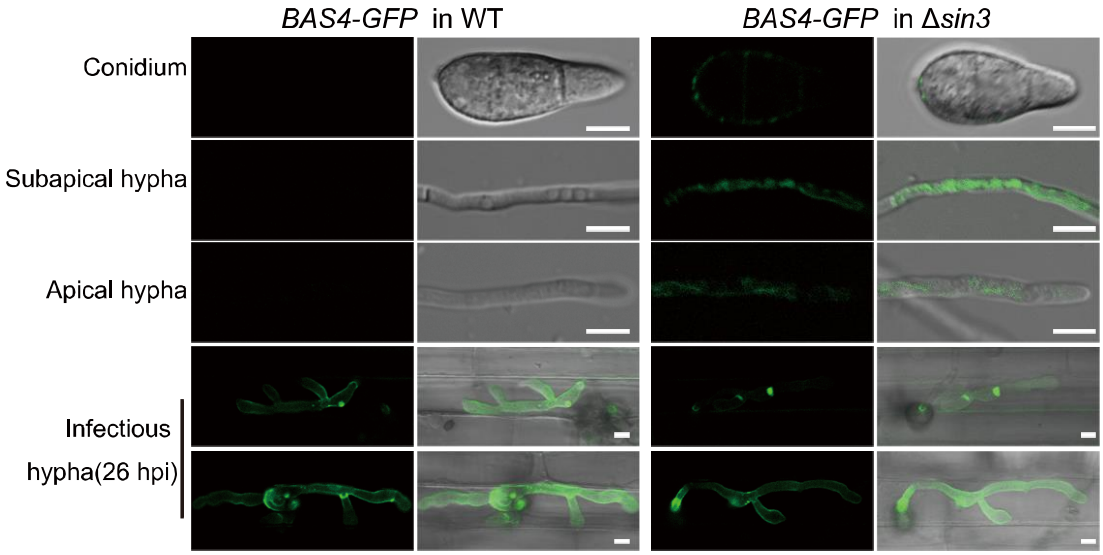

Figure S10. Confocal microscopy-based subcellular localization of Bas4-GFP in the vegetative and *in planta* growth stages in the WT and Δ*sin3* strains.

In the WT, Bas4-GFP fluorescence was only presented in the *in planta* growth stage, while in the Δ*sin3*, Bas4-GFP fluorescence could be detected during both vegetative and *in planta* growth stages, including the conidia, apical hypha, subapical hypha and invasive hypha. Bar = 5 μm.

Table S1. Components of polycomb repressive complex in *M. oryzae, N. crassa, A. thaliana,* and *D. melanogaster*.

Species	Subfamily	Protein name	Gene ID	GenBank accession numbers
Neurospora crassa	PRC2	NcSET-7	NCU07496	XP_965043.2
		NcEED	NCU05300	XP_962071.2
		NcSUZ12	NCU05460	XP_963451.3
		NcP55	NCU06679	XP_960994.2
Cryptococcus neoformans	PRC2	CnEzh2	CNAG_07553	XP_012047965.1
		CnMsl1	CNAG_03297	XP_012051157.1
		CnBnd1	CNAG_07433	XP_012049647.1
		CnEed1	CNAG_02345	XP_012050093.1
		CnCcc1	CNAG_00083	XP_012046514.1
Magnaporthe oryzae	PRC2	MoSET-7	MGG_00152	XP_003718975.1
		MoSUZ12	MGG_03169	XP_003716821.1
		MoEED	MGG_06028	XP_003711877.1
		MoP55	MGG_07323	XP_003715557.1
Arabidopsis thaliana	PRC2	AtCLF	AT2G23380	NP_179919.1
		AtMEA	AT1G02580	NP_563658.1
		AtSWN	AT4G02020	NP_567221.1
		AtFIE	AT3G20740	NP_188710.1
		AtEMF2	AT5G51230	NP_199936.2
		AtVRN2	AT4G16845	NP_567517.1
		AtFIS2	AT2G35670	NP_565815.2
		AtMSI1-5	AT5G58230	NP_200631.1
	PRC1	AtEMF1	AT5G11530	NP_196714.1
		AtRING1A	AT5G44280	NP_199241.2
		AtRING1B	AT1G03770	NP_171873.2
		AtLHP1	AT5G17690	NP_197271.1
		AtBMI1A	AT2G30580	NP_565702.1
		AtBMI1B	AT1G06770	NP_973775.1
		AtBMI1C	AT3G23060	NP_188946.2
Drosophila melanogaster	PRC2	DmEz	Dmel_CG6502	NP_524021.2
		DmESC	Dmel_CG14941	NP_477431.1
		DmSUZ12	Dmel_CG8013	NP_652059.1
		DmCaf	Dmel_CG4236	NP_524354.1
	PRC1	DmJARID2	Dmel_CG3654	NP_648324.1
		DmPCL	Dmel_CG5109	NP_476672.1
		DmPH	Dmel_CG18412	NP_476871.2
		DmPSC	Dmel_CG3886	NP_523725.2
		DmPC	Dmel_CG32443	NP_524199.1
		DmRing	Dmel_CG5595	NP_477509.1
		DmKDM2	Dmel_CG11033	NP_649864.2

Table S2. Primers used in this study.

Primer name	Sequence (5'-3')	Use
KMT6-5F	AATTGAATTC CGCATGGAGAACGTGCGATG	amplifying *KMT6* 5' flanking sequence for gene deletion (*pFGL821*)
KMT6-5R	AATTGGTACC GGCCTTGTCACTTTTGCTCCCT	
KMT6-3F	AATTCTGCAG GAGCAGTCGAGCGCACGGA	amplifying *KMT6* 3' flanking sequence for gene deletion
KMT6-3R	AATTAAGCTT CACCACGGTTGCTGGAGAGTACG	
SUZ12-5F	CGGAATTCCATCGTTGTCTCGGTGTTGC	amplifying *SUZ12* 5' flanking sequence for gene deletion (*pFGL821*)
SUZ12-5R	GGGGTACCTGGTGCGCTTAAGCATGAGA	
SUZ12-3F	AACTGCAGGCCCGAAACGTTCATACCAC	amplifying *SUZ12* 3' flanking sequence for gene deletion
SUZ12-3R	CCCAAGCTTTCTCGTGAAGAGAGTGCTGG	
EED-5F	CGGAATTCATTTCGGACTTCGGCACAGT	amplifying *EED* 5' flanking sequence for gene deletion (*pFGL821*)
EED-5R	GGGGTACCCGGTCCGATCCACGAAAAGA	
EED-3F	AACTGCAGTTGTCGCCGGGAGTAAGAAC	amplifying *EED* 3' flanking sequence for gene deletion
EED-3R	CCCAAGCTTCGAAATTCTGATGCGCGAGG	
P55-5F	CGGAATTCAATGAATGGGCGGGAGTCTG	amplifying *P55* 5' flanking sequence for gene deletion (*pFGL821*)
P55-5R	GGGGTACCTGCAATGGCCAATGAAACTCT	
P55-3F	AACTGCAGTGCCGAGTCGATCGTTAAGC	amplifying *P55* 3' flanking sequence for gene deletion
P55-3R	CCCAAGCTTTGTCGACCTTGTCAAGCTGTT	
SIN3-5F	GGAGAAACTCGAGAATTC TCAAGGCGAGTTAGGGCAG	amplifying *SIN3* 5' flanking sequence for gene deletion (*pFGL821*)
SIN3-5R	GAGTTCAGGCTTTTTCATATCTCGGAGAGGGTGGTTC	
SIN3-3F	TCCGAGGGCAAAGAAATAGCTTTGCAGTGACGAGCTGC	amplifying *SIN3* 3' flanking sequence for gene deletion
SIN3-3R	CAAGCTTGCATGCCTGCAGATTCTCGGTTGTGGCCCTC	
SAP18-5F	GGAGAAACTCGAGAATTCGTTGTAGGGATCGGCACG	amplifying *SAP18* 5' flanking sequence for gene deletion (*pFGL821*)
SAP18-5R	GAGTTCAGGCTTTTTCATGCAAGCGTCTTGATGTATT	
SAP18-3F	TCCGAGGGCAAAGAAATAGTCTGGGAAGCTGAGCTTT	amplifying *SAP18* 3' flanking sequence for gene deletion
SAP18-3R	CAAGCTTGCATGCCTGCAGGGAGTTAGGTGAAGCAAGTC	
SAP30-5F	GGAGAAACTCGAGAATTCAGTAGTGCTGGGTAAGCGATACCC	amplifying *SAP30* 5' flanking sequence for gene deletion (*pFGL821*)
SAP30-5R	GAGTTCAGGCTTTTTCATGTCTGGCTGGTGTGTATCTGGG	
SAP30-3F	TCCGAGGGCAAAGAAATAGCTGGGCGGTCTGGACATAGCTT	amplifying *SAP30* 3' flanking sequence for gene deletion
SAP30-3R	CAAGCTTGCATGCCTGCAGGGTCGAATCGCCCTATTTCCC	
SIN3bp-5F	GGAGAAACTCGAGAATTCAATTGCACTTGATCCAAT	amplifying *SAP30* 5' flanking sequence for gene deletion (*pFGL821*)
SIN3bp-5R	GAGTTCAGGCTTTTTCATGGGAGCAAGATGCCTCCG	
SIN3bp-3F	TCCGAGGGCAAAGAAATAGTCTGGGAAGCTGAGCTTT	amplifying *SAP30* 3' flanking sequence for gene deletion
SIN3bp-3R	CAAGCTTGCATGCCTGCAGAACGTATTTCACCAAGCTG	
HOS2-5F	AGTGAATTCTGAAGGAGGCTGGGAGATGAA	amplifying *HOS2* 5' flanking sequence for gene deletion (*pFGL821*)
HOS2-5R	AGTGGATCCGTACTTTGGGCTAAAGGTCAAAGG	
HOS2-3F	AGTGTCGACCAGAAGAGTCTTTCTCTTGCACCC	amplifying *HOS2* 3' flanking sequence for gene deletion
HOS2-3R	AGTAAGCTTGCCCTGGTCCCATATCCATTC	
KMT6-TF	AATCTCGTATAGAAGCACGCCTAGTT	transformants screening
KMT6-IN-F	GCCGCAGCTCGTAGCAACGC	
KMT6-IN-R	AGGGCCCGTCGTGTATGCAT	
SUZ12-TF	AACAGGCTCGTCTGGTATCAAGAGAA	transformants screening
SUZ12-IN-F	TTCCTTGACATAGAGAAGTGGCGTCT	
SUZ12-IN-R	GACATTGTCGCCGTAGAAGGAGAC	

EED-TF	AACCTGCTTACGACGAGCTGCTC	transformants screening
EED-IN-F	GGGCTACGTCGCCAAGATCAA	
EED-IN-R	ATGCGCCTTGTCACTAAGTTCCTT	
P55-TF	AAATGGGAACGTCATCCTACCATC	transformants screening
P55-IN-F	AACTATCGCATTCACCGTGTCCT	
P55-IN-R	GGCAAAAGTCTAGTGCGTTGATGG	
SIN3-TF	ATCGCCGCTATTATCGGCGA	transformants screening
SIN3-IN-F	CGGCTTCGTTGAATGGAAGTTCT	
SIN3-IN-R	TCATTGGTTCAGGCACAATGGG	
SAP18-TF	GAAGGCAGTTCTTCAGCGATG	transformants screening
SAP18-IN-F	GCGTTTCACAGGTTAGTGCTTTAC	
SAP18-IN-R	GCGACAGATCCGTCCTCCAGA	
SAP30-TF	GGCTCAGATATCGTTTTGGGCC	transformants screening
SAP30-IN-F	TCACGGCAATGGCAAGGACAA	
SAP30-IN-R	CGTTGCGACTTTGTGGACGAA	
SIN3bp-TF	GATTCGGTCGTATTGGTCGAGC	transformants screening
SIN3bp-IN-F	TCCCTGTGACCAAGAATCACCCT	
SIN3bp-IN-R	AACGACATCACCATTGATCCCAC	
HOS2-TF	CGACGAGTGTCTAGCCAGATTG	transformants screening
HOS2-IN-F	GACCTCAAGTTTAACCTCGGAGG	
HOS2-IN-R	GCCAAAGAGGATCATGGGAAT	
KMT6-GFP-5f	GCCGTTTACGGCAACCTCA	construction of *KMT6-GFP* and complementation (*pFGL820*)
KMT6-GFP-5r	AATTGGTACCAGGACCTCTACGATATCGTACAGG	
KMT6-com-if	GAGAATTCGAGCTCGGTACCGCTCGGTCGAGAATTGACTT	
KMT6-com-iR	GCAGGTCGACTCTAGATGGAACTTGTCGCGGAATAC	
SUZ12-c-5f	TATGGAGAAACTCGAGAATTCCATCGTTGTCTCGGTGTTGCG	construction of *SUZ12-GFP* and complementation (*pFGL820*)
SUZ12-c-5r	TGCTCACCATCAAGTCCACACAGTCATTACATAGCC	
SUZ12-GFP-Trpcf	TGTGGACTTGATGGTGAGCAAGGGCGAGG	
SUZ12-GFP-Trpcr	GACTCTAGAACTAGTGGATCCCGAGCCCTCTAAACAAGTGTACC	
SUZ12-c-3f	GAATTGCATGTCGACCTGCAGGGGCTATTGTAGCCGTGACTATC	
SUZ12-c-3r	ACGACGGCCAGTGCCAAGCTTTCTCGTGAAGAGAGTGCTGGAA	
EED-c-5f	TATGGAGAAACTCGAGAATTCATTTCGGACTTCGGCACAGTC	construction of *EED-GFP* and complementation (*pFGL820*)
EED-c-5r	CCCTTGCTCACCATTCTATGACTACCCTTTGGAACTGGT	
EED-GFP-Trpcf	CATAGAATGGTGAGCAAGGGCGAGG	
EED-GFP-Trpcr	GACTCTAGAACTAGTGGATCCCGAGCCCTCTAAACAAGTGTACC	
EED-c-3f	GAATTGCATGTCGACCTGCAGATCCGGGGTGTGTTTTTTGG	
EED-c-3r	ACGACGGCCAGTGCCAAGCTTCGAAATTCTGATGCGCGAG	
P55-c-5f	CGAGAATTCGAGCTCGGTACCAATGAATGGGCGGGAGTCTG	construction of *P55-GFP* and complementation (*pFGL820*)
P55-c-5r	TCCTCGCCCTTGCTCACCATGGGGCCCAGCTCGTCCAC	
P55-GFP-Trpcf	ATGGTGAGCAAGGGCGAGG	
P55-GFP-Trpcr	CGTTGGCACCTCGACTCTAGACGAGCCCTCTAAACAAGTGTACC	
P55-c-3f	GAATTGCATGTCGACCTGCAGAGGACGGTCCAGCTCCGA	

P55-c-3f	ACGACGGCCAGTGCCAAGCTTTGTCGACCTTGTCAAGCTGTTC	
P55-c-F	AGTCTCGAGAGCCCTGCCATTCGGTGTC	
P55-c-R	AGTGGATCCTGACAGACGTTTGTTGGTGGGA	
SIN3-GFP-F	TATTATGGAGAAACTCGAGAGCAAGGAAGCCCAGAAGCG	construction of *SIN3-GFP* and complementation (*pFGL820*)
SIN3-GFP-R	CACCATGGTACCGAGCTCTGCAGAAGACCCAGCACCG	
flagKMT6F	CGACGATAAGCTCGAGACGGGCAAGCTCGGTGCCCT	construction of *FLAG-KMT6* (*pFGL822*)
flagKMT6R	TGTTTGATGAGCTGGGTACCTCAAGGACCTCTACGATATC	
flagSUZ12F	CGACGATAAGCTCGAGACTCCGCACGGCTTCAGACG	construction of *FLAG-SUZ12* (*pFGL822*)
flagSUZ12R	TGTTTGATGAGCTGGGTACCTTACAAGTCCACACAGTCAT	
flagEEDF	CGACGATAAGCTCGAGGCCGGTGGCGACGCGTCGGG	construction of *FLAG-EED* (*pFGL822*)
flagEEDR	TGTTTGATGAGCTGGGTACCCTATCTATGACTACCCTTTG	
flagP55F	CGACGATAAGCTCGAGGCACCTCCTCCAGCCATGGA	construction of *FLAG-P55* (*pFGL822*)
flagP55R	TGTTTGATGAGCTGGGTACCCTAGGGGCCCAGCTCGTCCA	
flagSIN3F	TGACGACGATAAGCTCGAGATGAATTCTCAACGGTCCCACG	construction of *FLAG-SIN3* (*pFGL822*)
flagSIN3R	GGAACAAAAGCTGGGTACCTTATGCAGAAGACCCAGCACC	
flagSAP18F	TGACGACGATAAGCTCGAGATGATGGAGATGGACAGGAACG	construction of *FLAG-SAP18 (pFGL822*)
flagSAP18R	GGAACAAAAGCTGGGTACC TCAGGGGTATTTCCCGCGAT	
flagSAP30F	TGACGACGATAAGCTCGAGATGCCACCAGCAAAAGCACG	construction of *FLAG-SAP30* (*pFGL822*)
flagSAP30R	GGAACAAAAGCTGGGTACCTCAGTTCTTCCTGCGTGTTCTCG	
flagSIN3bpF	TGACGACGATAAGCTCGAGATGGCAACCATGGCAACTGCTAC	construction of *FLAG-SIN3* (*pFGL822*)
flagSIN3bpR	GGAACAAAAGCTGGGTACCTTATACAGAGCCGAGTTGAAGTAGAGC	
flagHOS2F	TGACGACGATAAGCTCGAGATGGATGCAGACTCATACAGATATCG	construction of *FLAG-HOS2* (*pFGL822*)
flagHOS2R	GGAACAAAAGCTGGGTACCTTAAAACTCCATGGCTTGACCAAC	
qBAS1-F	CCGTCTATCGCGGCTGAAGATTAT	amplifying *MoBAS1*for RT-PCR
qBAS1-R	CGGGTAATAATTCTCCACCCGTCTA	
qBAS2-F	AGGGAGTCTGCTCCAACGAAGTCG	amplifying *MoBAS2* for RT-PCR
qBAS2-R	TGCTTCTTGACCTGCTCCTTGGC	
qBAS3-F	TCCCAGACCACTTGCCGTACTCAG	amplifying *MoBAS3* for RT-PCR
qBAS3-R	CAGCGCCGTTCAGGTTGCAGA	
qBAS4-F	GCTCAAGAAGAACGGCAAATGCG	amplifying *MoBAS4* for RT-PCR
qBAS4-R	GGGATAGACGAGCCAGTAGCGCC	
qSPD5-F	TTAACTTCTTCGGCCACAAGACG	amplifying *MoSPD5* for RT-PCR
qSPD5-R	GAGGCCGTCGTATTTGCAGTCCTC	
qSPD8-F	AGGGACGGTACGAAATTCGACACG	amplifying *MoSPD8* for RT-PCR
qSPD8-R	GGCCGCGATATTCCGAGGTCT	
qSPD10-F	CAAGGCCACCAACACCGACCT	amplifying *MoSPD10* for RT-PCR
qSPD10-R	TGCAGGCCCTTTGCAGGTTCT	
qAvr-PiK-F	CAACCCTGGTATTCCTGTACCCGAAT	amplifying *MoAvr-PiK* for RT-PCR
qAvr-PiK-R	CCCAGTTTGGACCAACTTTCATGTC	
qAvr-PiZt-F	CCAAAGAGGCTGGTCGCGATT	amplifying *MoAvr-PiZt* for RT-PCR
qAvr-PiZt-R	GAGAGAACATCAGTGGACGTCCC	
qAvr-Pi9-F	GGCCGAAGGTGACGCCAAGAT	amplifying *MoAvr-Pi9* for RT-PCR
qAvr-Pi9-R	TTGGCACCAGCCATCATCGCA	
qACE1-F	GAGGGCACCAATAGCCTCGACCT	amplifying *MoACE1* for RT-PCR

qACE1-R	CAGCGACGTTCTCGACCGACAC	
qHEG13-F	TTGCTCACCAAACGGTCACACG	amplifying *MoHEG13* for RT-PCR
qHEG13-R	TGGTTGTCCGGCAACACGTTG	
qβ-Tubulin-F	CTGCCATCTTCCGTGGAAAGG	analysis the expression level of *β-tubulin* gene of *M.oryzae*
qβ-Tubulin-R	GACGAAGTACGACGAGTTCTTG	
ChIP-qMPG1-F	ACTAACTGACTGAGTGACTGAGGGACTT	amplifying *MoBAS1*for ChIP-qPCR
ChIP-qMPG1-R	GTGAGCTTTGGGATGATGAGAAGAG	
ChIP-BAS3-F	CTTGAAGACAGACCAGCAAATCGC	amplifying *MoBAS2* for ChIP-qPCR
ChIP-BAS3-R	ATGGCAAAGGAGACGGTGGAGA	
ChIP-BAS4-F	CTCATTCTCAGCAATCGCCATCC	amplifying *MoBAS3* for ChIP-qPCR
ChIP-BAS4-R	TCTGCACTGTTGTTGTCGGGGTA	
ChIP-SPD5-F	CCAGACATATCTACCACCAAGAAGGC	amplifying *MoBAS4* for ChIP-qPCR
ChIP-SPD5-R	ATGGCGGCAATGTGGAGGATT	
ChIP-SPD10-F	CACCCGCAACGACAAAAAAGC	amplifying *MoSPD5* for ChIP-qPCR
ChIP-SPD10-R	CCAGGAGCAAGGGGAGAACGA	
ChIP-Tub5-F	GTTGCAGCTAGCACAGACCA	amplifying *Moβ-tubulin*for ChIP-qPCR
ChIP-Tub5-R	GTCGGGATTGATTGGATTTG	
AD-KMT6F	GCCATGGAGGCCAGTGAATTCATGACGGGCAAGCTCGGT	construction of AD-*KMT6* (pGADT7)
AD-KMT6R	CAGCTCGAGCTCGATGGATCCTCAAGGACCTCTACGATATCGTACA	
BD-KMT6F	ATGGCCATGGAGGCCGAATTCATGACGGGCAAGCTCGGT	construction of BD-*KMT6* (pGBKT7)
BD-KMT6R	CCGCTGCAGGTCGACGGATCCTCAAGGACCTCTACGATATCGTACA	
AD-SUZ12F	GCCATGGAGGCCAGTGAATTCATGACTCCGCACGGCTTCA	construction of AD-*SUZ12* (pGADT7)
AD-SUZ12R	CAGCTCGAGCTCGATGGATCCTTACAAGTCCACACAGTCATTACATAGC	
BD-SUZ12F	ATGGCCATGGAGGCCGAATTCATGACTCCGCACGGCTTCA	construction of BD-*SUZ12* (pGBKT7)
BD-SUZ12R	CCGCTGCAGGTCGACGGATCCTTACAAGTCCACACAGTCATTACATAGC	
AD-EEDF	GCCATGGAGGCCAGTGAATTCATGGCCGGTGGCGACGCG	construction of AD-*EED* (pGADT7)
AD-EEDR	CAGCTCGAGCTCGATGGATCCCTATCTATGACTACCCTTTGGAACTGG	
BD-EEDF	ATGGCCATGGAGGCCGAATTCATGGCCGGTGGCGACGCG	construction of BD-*EED* （pGBKT7)
BD-EEDR	CCGCTGCAGGTCGACGGATCCCTATCTATGACTACCCTTTGGAACTGG	
BD-P55F	ATGGCCATGGAGGCCGAATTCATGGCACCTCCTCCAGCC	construction of BD-*P55* （pGBKT7)
BD-P55R	CCGCTGCAGGTCGACGGATCCCTAGGGGCCCAGCTCGTC	
AD-P55F	GCCATGGAGGCCAGTGAATTCATGGCACCTCCTCCAGCC	construction of AD-*P55* (pGADT7)
AD-P55R	CAGCTCGAGCTCGATGGATCCCTAGGGGCCCAGCTCGTC	
AD-SIN3F	GCCATGGAGGCCAGTGAATTCATGAATTCTCAACGGTCCCACG	construction of AD-*SIN3* (pGADT7)
AD-SIN3R	CAGCTCGAGCTCGATGGATCCTTATGCAGAAGACCCAGCACC	
AD-SAP18F	GCCATGGAGGCCAGTGAATTCATGATGGAGATGGACAGGAACG	construction of AD-*SAP18* (pGADT7)
AD-SAP18R	CAGCTCGAGCTCGATGGATCCTCAGGGGTATTTCCCGCGAT	
AD-SAP30F	GCCATGGAGGCCAGTGAATTCATGCCACCAGCAAAAGCACG	construction of AD-*SAP30* (pGADT7)
AD-SAP30R	CAGCTCGAGCTCGATGGATCCTCAGTTCTTCCTGCGTGTTCTCG	
AD-SIN3bpF	GCCATGGAGGCCAGTGAATTCATGGCAACCATGGCAACTGCTAC	construction of AD-*SIN3bp* (pGADT7)
AD-SIN3bpR	CAGCTCGAGCTCGATGGATCCTTATACAGAGCCGAGTTGAAGTAGAGC	
AD-HOS2F	GCCATGGAGGCCAGTGAATTCATGGATGCAGACTCATACAGATATCG	construction of AD-*HOS2* (pGADT7)
AD-HOS2R	CAGCTCGAGCTCGATGGATCCTTAAAACTCCATGGCTTGACCAAC	

Table S3. Strains used in this study.

Strain	**Genotype description**
B157	Wild-type
Δ*kmt6*	deletion mutant of *MGG_00152* in B157
Δ*kmt6*-C	expressing *KMT6-GFP* in Δ*kmt6* transformant
Δ*suz12*	deletion mutant of *MGG_03169* in B157
Δ*suz12*-C	expressing *SUZ12-GFP* in Δ*suz12* transformant
Δ*eed*	deletion mutant of *MGG_06028* in B157
Δ*eed*-C	expressing *EED-GFP* in Δ*eed* transformant
Δ*p55*	deletion mutant of *MGG_07323* in B157
Δ*p55*-C	expressing *P55-GFP* in Δ*p55* transformant
Δ*sin3*	deletion mutant of *MGG_13498* in B157
Δ*sin3*-C	expressing *SIN3-GFP* in Δ*sin3* transformant
Δ*sap18*	deletion mutant of *MGG_05680* in B157
Δ*sap30*	deletion mutant of *MGG_11142* in B157
Δ*sin3bp*	deletion mutant of *MGG_10153* in B157
Δ*hos2*	deletion mutant of *MGG_01633* in B157
P55-FLAG	*pRP27-P55-FLAG* in Δ*p55* transformant
SUZ12-FLAG	*pRP27-SUZ12-FLAG* in Δ*suz12* transformant
KMT6-FLAG	*pRP27-KMT6-FLAG* in Δ*kmt6* transformant
SIN3-FLAG	*pRP27-SIN3-FLAG* in Δ*sin3* transformant
EED-FLAG	*pRP27-EED-FLAG* in Δ*eed* transformant
SAP18-FLAG	*pRP27-SAP18-FLAG* in Δ*sap18* transformant
HOS2-FLAG	*pRP27-HOS2-FLAG* in Δ*hos2* transformant
SUZ12-GFP/KMT6-FLAG	*pRP27-P55-FLAG* in *KMT6-FLAG* transformant
P55-GFP/KMT6-FLAG	expressing *P55-GFP* in *KMT6-FLAG* transformant
P55-GFP/SUZ12-FLAG	expressing *P55-GFP* in *SUZ12-FLAG* transformant
P55-GFP/EED-FLAG	expressing *P55-GFP* in *EED-FLAG* transformant
P55-GFP/SIN3-FLAG	expressing *P55-GFP* in *SIN3-FLAG* transformant
P55-GFP/SAP18-FLAG	expressing *P55-GFP* in *SAP18-FLAG* transformant
P55-GFP/HOS2-FLAG	expressing *P55-GFP* in *HOS2-FLAG* transformant
Guy11	Wild-type
Δ*kmt6(*Guy11)	deletion mutant of *MGG_00152* in Guy11